Engineering Structures 257 (2022) 114096

Contents lists available at ScienceDirect

Engineering Structures

journal homepage: www.elsevier.com/locate/engstruct

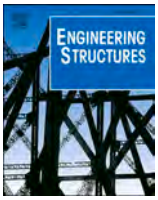

Experimental investigation of wind impact on low-rise elevated residences

Nourhan Abdelfatah [a], Amal Elawady [a,b,*], Peter Irwin [a,b], Arindam Gan Chowdhury [a,b]

[a] The Department of Civil and Environmental Engineering, Florida International University Miami, FL, USA
[b] The Wall of Wind Experimental Facility, Miami, FL, USA

ARTICLE INFO

Keywords:
Aerodynamics
Elevated structure
CFD
Experimental
Peak pressure
Residential buildings
Stilt
Wall of Wind

ABSTRACT

The vulnerability of low-rise residential buildings to extreme wind events, such as hurricanes, is an escalating concern due to the frequent failures and losses. Elevated low-rise structures are constructed to reduce the hydrodynamic load from surges and flooding during hurricanes. However, due to the current lack of information, wind loading on elevated coastal structures is not adequately addressed in current international guidelines. To address this knowledge gap, large-scale experimental studies were conducted to precisely determine wind effects on elevated houses with different numbers of stories and varying stilt heights. In this study, comparisons are presented on various tested configurations to show the effect of elevating residential houses on the resulting wind loads. In particular, this work investigates the peak pressure coefficients and wind forces on the building roof, walls, and floor underside. The experimental program was supplemented by numerical simulations using Computational Fluid Dynamics (CFD) to assess the airflow around the model and the role of the air gap underneath the floor on altering the aerodynamics. Local peak pressure patterns and wind loads for structural design were analyzed with a view to the development of building code provisions. The recommended external pressure coefficients for the exterior floor surface are compared to those for a flat roof surface of a low-rise building.

1. Introduction

Coastal regions have for many years experienced large increases in population and business migration. Almost 40% of the world's population lives 100 km or less from the coast, according to the United Nations [2]. In 1996, Hinrichsen estimated that by 2025 approximately 70% of the world population would live 200 km from the shoreline [3]. The infrastructure, residential developments and population density in these areas are rapidly increasing. Yet, concerns about the impacts of combined wind and wave hazards on the resiliency of coastal communities remain unresolved, especially with the increasing occurrence of extreme wind events. The National Oceanic and Atmospheric Administration (NOAA) [4] has published tropical cyclone records since 1851 in the Atlantic Ocean, the Caribbean Sea, and the Gulf of Mexico. Statistical analyses showed a total increase of 36% in the number of storms over the past 50 years. In addition, currently, there is a 50% probability that ten storms will occur per year [5]. Hurricanes (Harvey, Irma, and Maria) in 2017 resulted in insurance claims that exceeded $265B [6–8]. In 2018, Hurricane Michael's landfall near Mexico Beach, FL, impacted the region with wind speeds exceeding 150 mph and a storm surge exceeding 6 ft, causing insurance losses of more than $7.2 billion in Florida alone [9,10].

Furthermore, in 2019, Hurricane Dorian, which hit the Bahamas, resulted in insured losses of about $6.5 billion [11]. In 2020, the coastal areas of the US were hit by Hurricanes Sally, Laura, and Delta. The insured losses were estimated to be more than $15 billion for Hurricane Laura alone [12,13].

A traditional approach to reduce the impact of hurricane-induced surge and flood loads on coastal structures is elevating houses above the ground level using stilts. Elevating residential houses to the Base Flood Elevation (BFE) is an effective way to avoid flood hazards [14,15]. However, damage assessment studies in the wake of recent hurricanes demonstrate elevated homes remain vulnerable to wind hazards. Elevating a building on stilts changes its structural properties and exposes the building to higher wind intensity [16,17]. Numerous coastal buildings have experienced considerable wind-induced damages during recent hurricanes, including roof and wall cover loss [18,19]. Amini and Memari showed several modes of damage experienced by elevated

* Corresponding author at: The Department of Civil and Environmental Engineering, Florida International University, 10555 W. Flagler Street, EC 3629 Miami, FL, USA.
E-mail address: aelawady@fiu.edu (A. Elawady).

https://doi.org/10.1016/j.engstruct.2022.114096
Received 16 July 2021; Received in revised form 28 January 2022; Accepted 2 March 2022
Available online 12 March 2022

Fig. 1. A post-hurricane survey photo of a one-story elevated house located in Abaco Island shows the wall and roof damage caused by hurricane Dorian in 2019 [1].

houses during Hurricane Michael [5]. This survey showed that the most common failure mode is the wall and roof cladding. Fig. 1 displays the roof and wall damage of a one-story elevated house located in Abaco Island, Bahamas, after the impact of Hurricane Dorian. This structure is located 150 m away from the shoreline. The severe damage displayed is believed to be a result of high-intensity wind and wind-borne debris impact.

Fig. 2a-b present a typical wall and roof cladding damage observed on two-story residential houses recorded after the passage of hurricanes Sally and Laura, respectively. The gable-roof elevated house shown in Fig. 2a is located 300 m away from Alabama's southern coast. More than 50% of the building cladding has been removed due to Hurricane Sally's passage. The building shown in Fig. 2b was hit by Hurricane Laura which caused severe damage to the roof and wall cladding. Despite the severity and destructive effects, there are only a few studies in the literature of the wind impact on elevated coastal buildings.

Holmes studied the effect of elevating a tropical house on the resulting surface pressure distribution [20]. The author tested on-ground and elevated models using small-scale (1:100) models. The study showed an increase of 30% of the wall mean pressure coefficients and slight differences on the roof surface compared to the on-ground counterpart. Amini and Memari surveyed the performance of several coastal houses impacted by recent hurricanes [21]. The study recommended considering the new aerodynamics of elevated houses while retrofitting to resist higher levels of wind forces. An ongoing experimental study is being conducted at the Natural Hazard Engineering Research Infrastructure (NHERI) Wall of Wind (WOW) Experimental Facility (EF) to assess the wind effects on coastal houses with different elevations [22,23]. The study used four 1:5 large-scale aerodynamic tests to evaluate the peak pressure distributions on the model surfaces. The study included an on-ground case, a mobile home case (0.6 m elevation), and two typical elevated cases (2.15 m and 3.6 m elevation). The use of large-scale models was to reduce expected Reynolds number (Re) effects and increase the reliability of peak pressure values [24,25]. Abdelfatah et al. showed slight differences in the roof peak pressure coefficients and higher pressure coefficients on the wall surface compared to the on-ground case [22], which agrees with the findings reported by Holmes 1994 [20]. A considerable increase of pressure coefficients was observed at the floor surface going from the 0.6 m elevation (mobile home) case to a 2.15 m elevated house case. The study recommended testing more configurations and a different number of stilts. Amini and Memari conducted a parametric numerical study to evaluate the effect of elevating the structure on the resulting mean pressure coefficients using Computational Fluid Dynamics (CFD) simulations [26]. The study adopted the models tested by Holmes to investigate more elevations and the wind flow characteristics. The author simulated a 1:20 on-ground and elevated (by 2.1 m and 4.2 m (full scale)) gable roof building. The results showed a slight increase in the suction coefficients occurring on the roof surface. The author stated that the increase of the pressure coefficients over the model surfaces caused an increase of 50% and 95% in the overturning moment acting on the 2.1 m and 4.2 m elevated cases, respectively, compared to the on-ground case.

Very limited information is available in current international standards for the design of elevated structures. To the authors' best knowledge, the provided coefficients to calculate wind loads are not given for a wide range of stilt cases and are not explained in detail. For example, the American standard (ASCE 7-16, 2016) provides external pressure coefficients for the edge and middle zones of the underside of elevated tanks or silos [27]. However, there is no recommendation for different elevations or geometrical changes. Besides, these values are recommended for cylindrical structures, which is not applicable for box buildings. But, draft provisions are under consideration to be published in ASCE 7-22. The Australian and New Zealand standard AS/NZS1170.2 [28] recommends using the same pressure coefficient for the windward walls of elevated or non-elevated cases. For the floor surface, AS/NZS standard recommends an averaged pressure coefficient value depending on the stilt's height.

A new phase of the research at the WOW EF includes an investigation of the effect of increasing the number of stories and increasing the stilt heights on the overall wind actions on elevated buildings. This study aims to deliver a better understanding and to further reduce the current knowledge gap related to wind impacts on elevated coastal buildings. One-story and two-story gable roof residential houses were tested using four different stilt heights. Compared to the results published earlier by Abdelfatah et al. [22], some adjustments were made in the current test phase to enhance the quality of the test and the results. The pressure taps were densified over the model surfaces, and an intermediate column was added in the middle of the longest span. The test program considered the maximum stilt height used for coastal houses according to FEMA

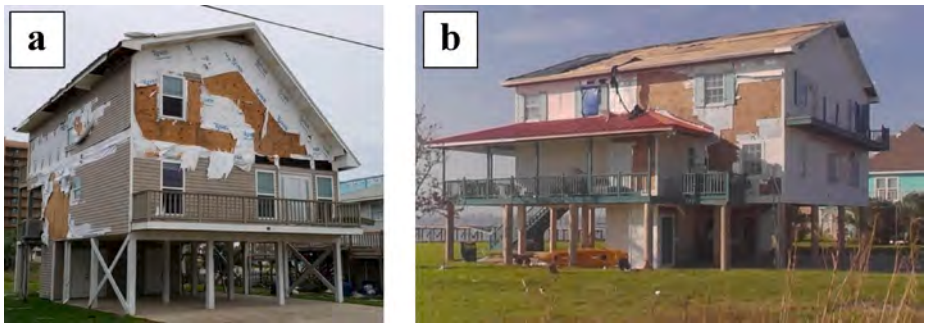

Fig. 2. Post-hurricane survey photos of two-story elevated houses which sustained wall and roof cladding damage in 2020 (a) Hurricane Sally, and (b) Hurricane Laura [1].

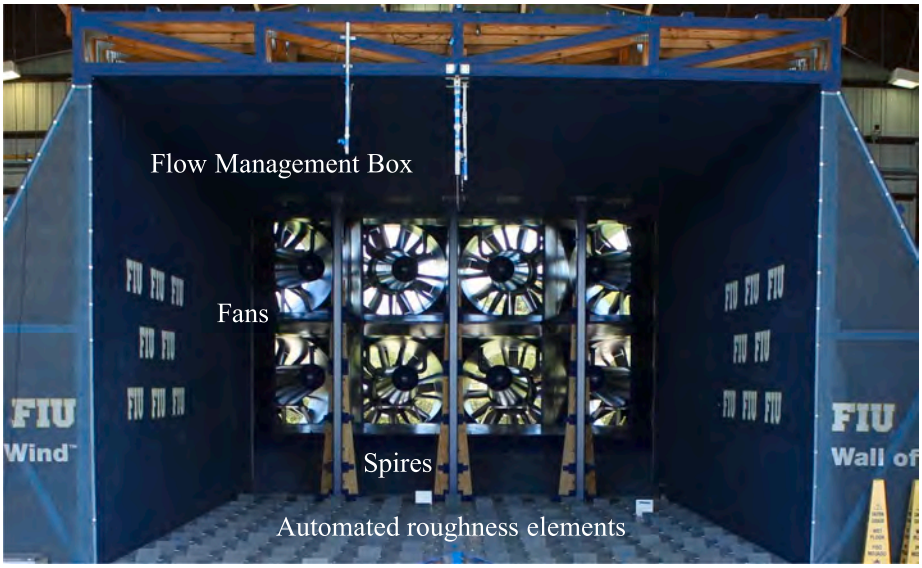

Fig. 3. A photo taken inside Wall of Wind facility showing the 12-fans intake inside the flow management box with automated roughness elements and spires.

Table 1
Model dimensions of the eight tested models and the Reynolds Number for each case (scale 1:5).

	Case number	Eave height (h)	Stilt height (S_h)	Reynolds Number
One-story	1S-0	64 cm	0 cm	1.12×10^6
	1S-43	64 cm	43 cm	1.28×10^6
	1S-73	64 cm	73 cm	1.32×10^6
	1S-104	64 cm	104 cm	1.38×10^6
Two-story	2S-0	110 cm	0 cm	2.00×10^6
	2S-43	110 cm	43 cm	2.11×10^6
	2S-73	110 cm	73 cm	2.21×10^6
	2S-104	110 cm	104 cm	2.23×10^6

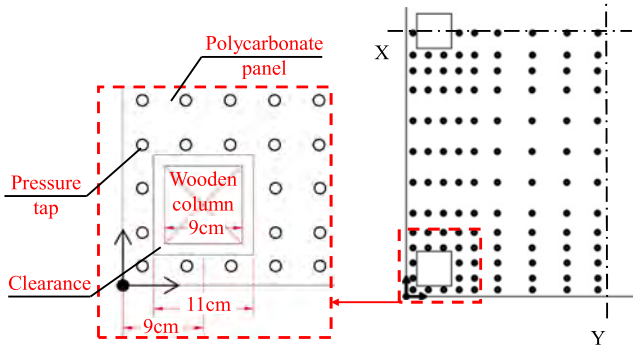

Fig. 4. 3D schematic of the tested model with the pressure taps' location, dimensions, and wind direction.

recommendations [14] and recent post-hurricane damage surveys [1]. The tested models were numerically simulated using CFD to present the flow characteristics for each case and visualize the effect of the air gap beneath the model. In this article, Section 2 describes the test setup and the analysis strategy in detail. In Section 3, flow streamline plots are provided, and the flow characteristics are discussed. Subsequently, contour plots of local peak pressure coefficients are presented. Also, a discussion on the differences between area-averaged pressure coefficients obtained from the experimental data and those available in national and international standards for the on-ground case is provided for the roof and walls. The area-averaged pressure coefficients on the floor surface are provided. To better understand the variation of wind loads with the variation of the house elevation, mean wind forces on the model surfaces are calculated and presented in Section 3.4.

2. Experimental procedures

The experimental program included two main cases; (1) a one-story house and (2) a two-story house. In each case, the model was adjusted to four different elevations, including an on-ground case. The model dimensions were selected to be similar to those typical of elevated houses damaged during recent hurricane incidents. The model stilt heights were selected to simulate realistic conditions of tropical houses as recommended by the Federal Emergency Management Agency [14]. In this section, the model configuration, test procedures, and instrumentations are described.

2.1. Testing facility

The testing was performed at the NHERI Wall of Wind (WOW) Experimental Facility (EF). The WOW is equipped with 12 fans, which can produce a wind speed of up to 70 m/s (i.e., category-five hurricane according to Saffir Simpson scale) [29,30]. Fig. 3 shows a view inside the flow management box and displays the arranged automated roughness elements and the vertical spires. These flow controllers can be adjusted to simulate the desired terrain category flow. In the current study, the tested model was placed on the 5 m diameter automated turntable which can rotate 360°.

2.2. Model setup and instrumentation

A typical low-rise gable roof model was adopted for this study. The prototype horizontal dimensions were 8.76 m long, and 6.4 m wide. The model aspect ratio matches typical damaged coastal houses observed through recent post-hurricane surveys [1]. For the on-ground one-story and two-story cases, the model eave heights were 3.2 m and 5.5 m, respectively. The roof pitch slope was 18°. In both test cases, the model was tested on-ground and elevated with three different heights (full-scale): 2.15 m, 3.65 m, and 5.2 m.

A length scale of 1:5 chosen for this experiment enabled the model to be adequately accommodated on the turntable. It also allowed the blockage ratio to be less than 5%, thereby keeping blockage effects to within acceptable levels [31]. In addition, the large length scale chosen for this test enabled a relatively high Reynolds number of about 2.2 ×

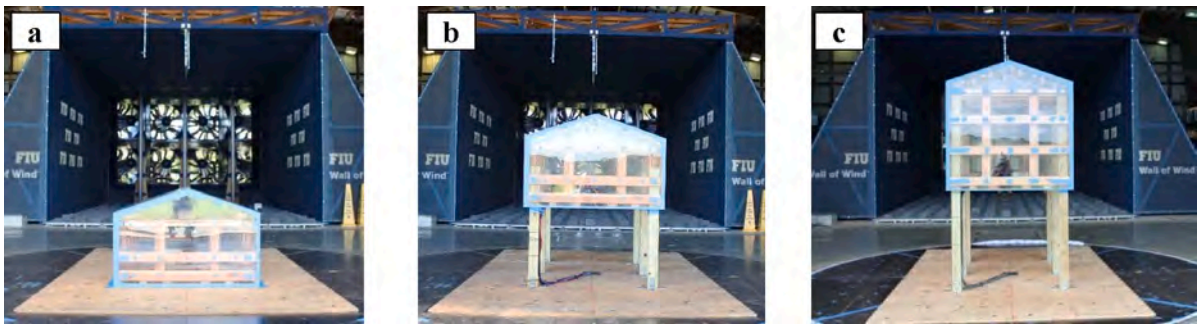

Fig. 5. Pressure taps distribution on the floor surface and around the stilt of the scaled model.

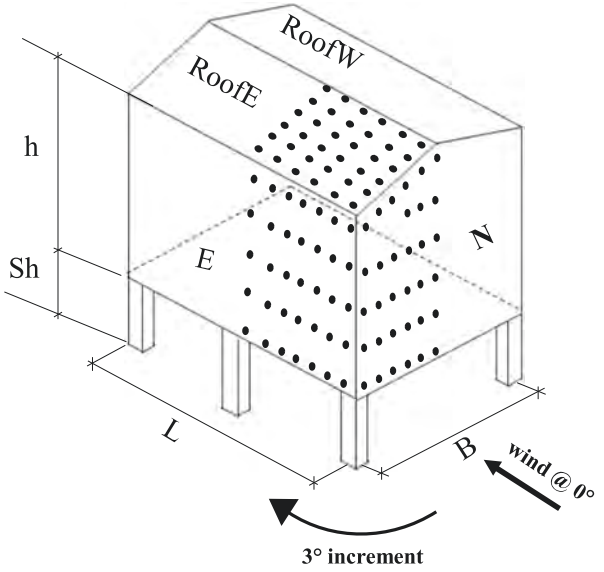

Fig. 6. Photos are taken inside Wall of Wind facility during the test of different cases of the scaled model (a) one-story on-ground case (1S-0), (b) elevated one-story case (1S-73), and (b) elevated two-story case (2S-104).

10^6 to be achieved. Table 1 shows the Reynolds number, for each of the tested models, calculated using the building height as a characteristic linear and the mean wind speed of each case. The model dimensions were similar to the previously tested models reported by Abdelfatah et al. [22]. However, some changes were done in this study to follow coastal houses' construction recommendations [14]. The long span was divided into two spans using two intermediate columns (Fig. 4). In addition, the pressure taps were distributed in a more dense pattern, especially on the floor surface (Fig. 5).

As shown in Fig. 6, the scale model was constructed using wooden frames. In the elevated cases, six 9 cm (representing 45 cm stilt's size in full scale) wooden members were used to raise the model to the desired heights. 9-mm thick polycarbonate panels covered the surfaces of the test models. Table 1 lists the eight model cases and their descriptions; moving forward in this manuscript, 1S will be used to describe one-story cases, while 2S will be used to describe two-story cases. A slight shift from the edge, 4.5 cm in the scale model, was left at the outer side of each stilt, as shown in Fig. 5. Stilts used in elevated buildings are typically constructed with this small shift from the edges, according to FEMA [14]. All the model cases were tested for a wind direction range 0–360° with 3° increment.

During the test, the WOW fans were adjusted to produce a mean wind speed of 25 m/s at 2 m height. The roughness elements and the WOW spires were adjusted to produce the wind profile of the open terrain category. Cobra probes were installed at different heights, including the mean roof height (MRH) of each tested case (e.g., 75 cm for 1S-0, 117 cm for 1S-43, 148 cm for 1S-73, and 178 cm for 1S-104). As shown in Fig. 7a, cobra probes were used to measure the wind velocity components before placing the model on the turntable. A sampling frequency of 2,500 Hz was used for the cobra probe measurements.

The one-story and the two-story models were instrumented with 262 and 307 pressure taps, respectively. Due to the building symmetry, those taps were distributed along one-quarter of the model roof walls and floor. The pressure taps were connected to a total of six Scanivalve

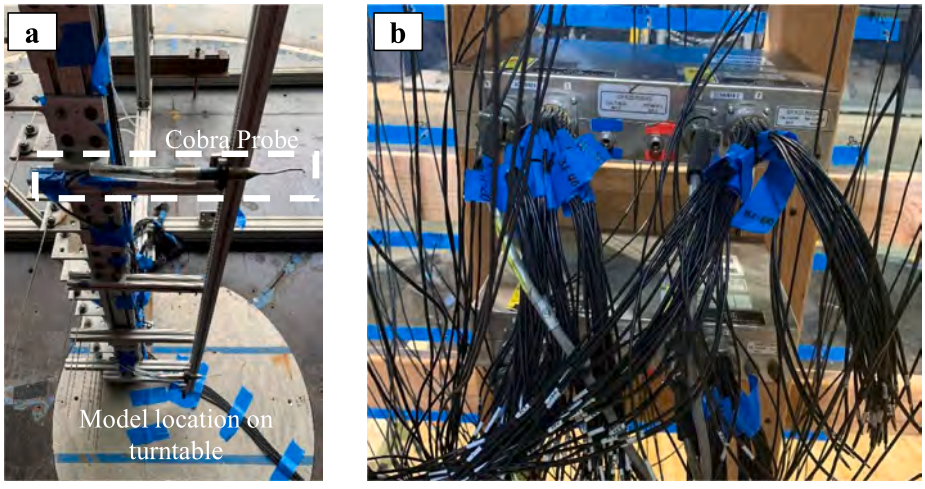

Fig. 7. Test instrumentations used during the test (a) Cobra probes for measuring 3-dimensional wind characteristics, and (b) Scanivalve ZOC33 connected to the model pressure taps.

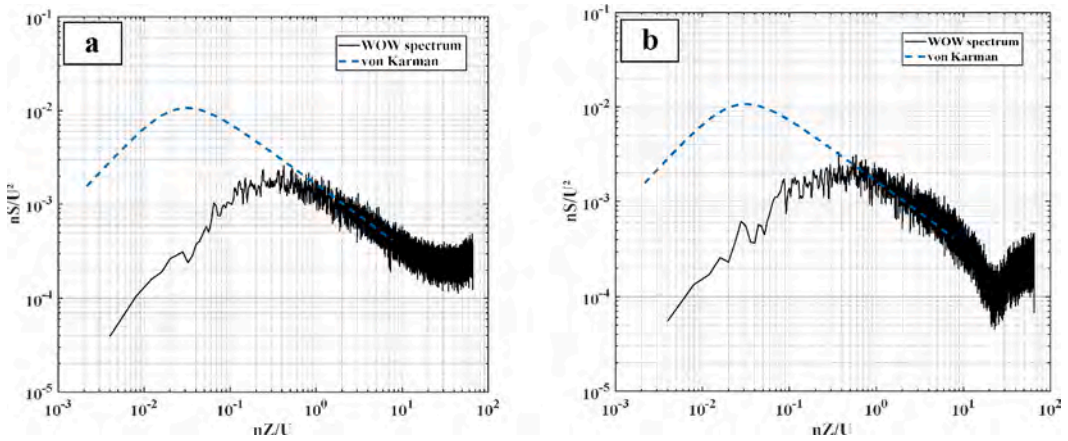

Fig. 8. Turbulence power spectra inside WOW compared to von Karman spectrum (a) case 2S-0, and (b) case 1S-43.

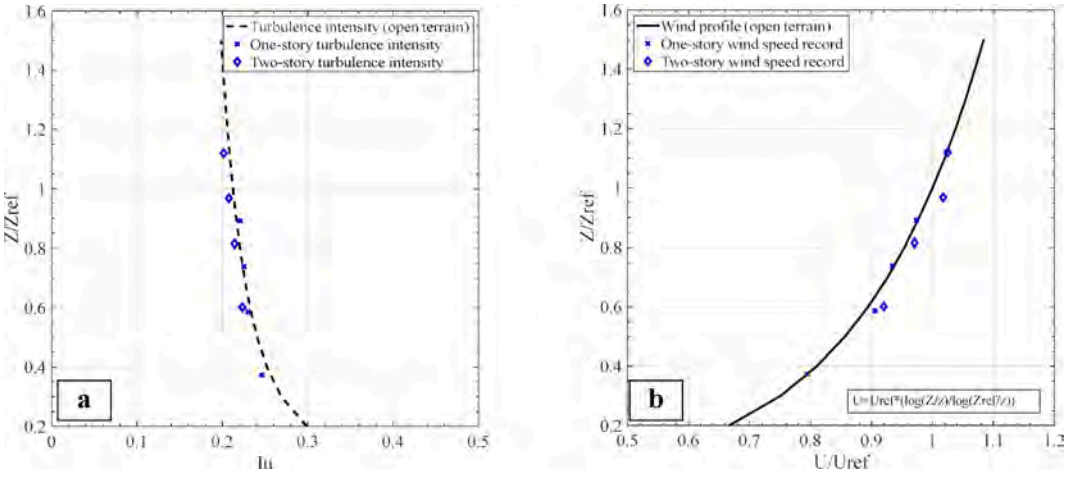

Fig. 9. Atmospheric Boundary Layer in WOW compared to full-scale wind profile [33] (a) Turbulence intensity, and (b) Normalized mean wind speed.

ZOC33 pressure scanners using flexible tubes, as shown in Fig. 7b. The tubes used for pressure sampling were 1.2 m in length and their inner diameter is 1.3 mm. Pressure data were recorded with a sampling rate of 520 Hz for 60 s.

2.3. Data analysis

As mentioned earlier, the WOW fan, spires, and automatic roughness elements were adjusted so that the post-test analysis results represented those applicable in open terrain conditions. The fluctuation of wind speed in three directions was recorded for 180 s at the model location. The wind speed (U) and the turbulence intensity (I_u) were calculated for each height (Z).

As expected, the relatively long length of the pressure tubing caused some distortion during pressure-time history data collection. The distortion of pressure signals caused by the tubing was compensated for using the inverse transfer function method described by Irwin et al. [32], and a low pass filter at 250 Hz was applied. The Transfer Function caused the deviation RMS between the long tubing data and short tubing data to be $2x10^{-4}$. Finally, Equation (1) was used to calculate the pressure coefficients.

$$C_P = \frac{P}{\frac{1}{2}\rho V^2} \quad (1)$$

where ρ is the density of air, P is the peak differential pressure (the difference between the model surface and the reference pressure), V is the 3-s gust wind speed at the mean roof height for each stilt case.

The limited test section size impedes the ability to form large eddies with respect to the model size. As a result, a deficiency in the low-frequency content of the wind tunnel spectrum occurs and, unless compensated for, would lead to an underestimation of peak pressure coefficient values. Fig. 8a-b shows the non-dimensional longitudinal turbulence power spectra of the WOW measured flow at the mean roof height of each model (z) versus the Engineering Sciences Data Unit (ESDU) [33], full-scale normalized longitudinal turbulence spectral density for the coastal region. In the plot, the frequency is denoted as n (Hz), the turbulence power spectrum is denoted as S. These figures illustrate the missing low-frequency part for 2S-0 and 1S-43 cases, respectively. In both cases, the wind speed was recorded at almost the same height (6 m in full scale). To ensure the accuracy of the estimated peaks, the partial turbulence simulation (PTS) method was used to compensate for missing low-frequency content in the peak estimation process.

PTS method is based on quasi-steady theory assumptions. The method depends on the match of the non-dimensional power spectrum of the longitudinal turbulence for the large-scale model and the full-scale spectrum for the high frequencies. Then, assuming a Gaussian probability distribution for the low-frequency turbulence, the PTS

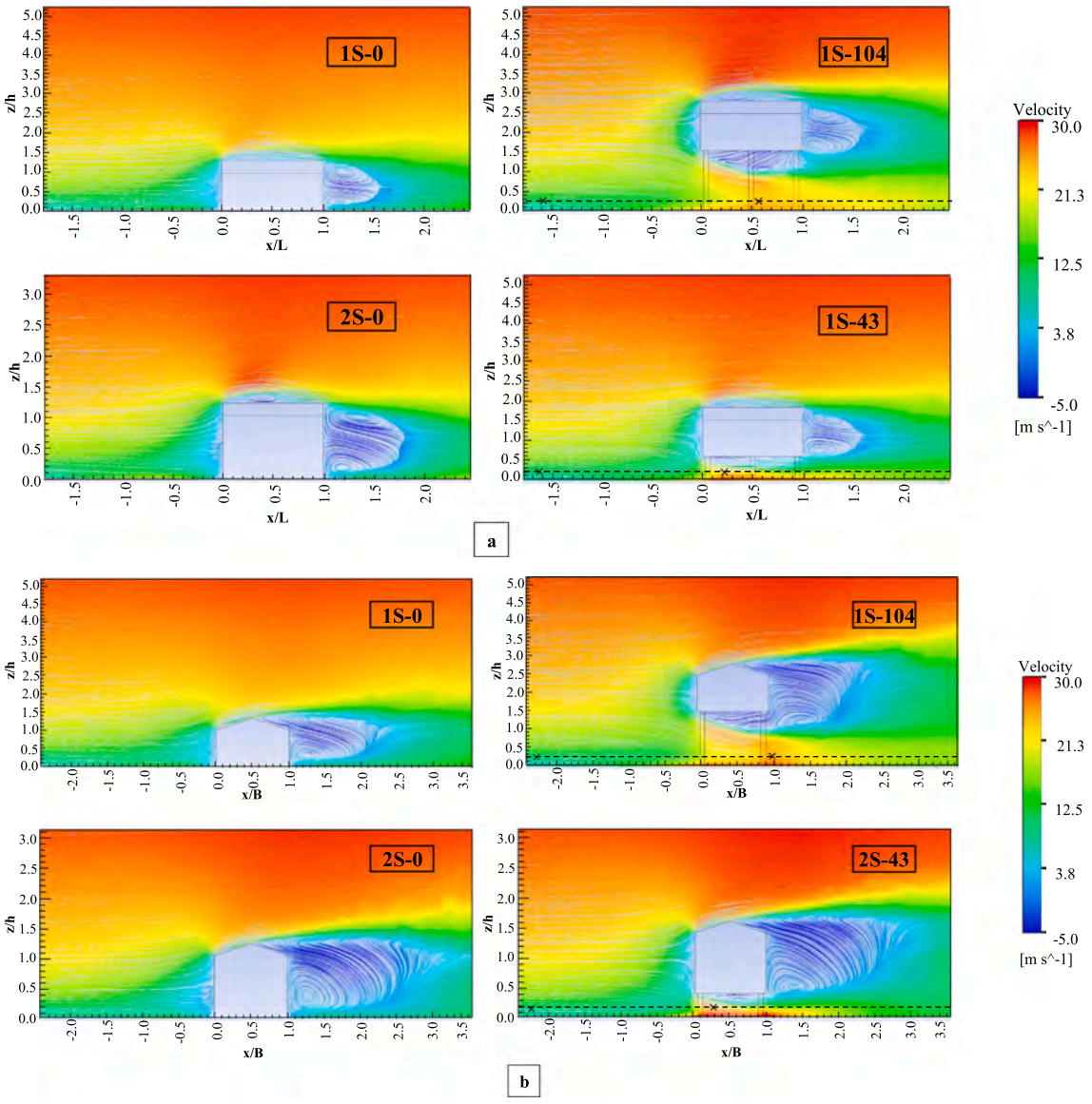

Fig. 10. Airflow streamlines at midspan section of the numerical model using CFD (a) 0° wind direction, and (b) 90° wind direction.

method combines the low-frequency effects with the high-frequency data obtained in the wind tunnel in order to include the entire spectrum. The peak pressure coefficients can be estimated by dividing the sample period into subintervals where peak values could be treated as independent. Each subinterval has its own peak value. And the probability that this peak will not be exceeded in 1 h at full scale is set at 0.78. Fig. 8 shows that at high frequencies of the model spectrum and the full-scale spectrum successfully match each other. After adjusting the resulting pressure coefficients using the PTS method, the peak values were calculated at full scale. Fig. 9a shows the turbulence intensity (I_u) at the MRH of each case after adding the missing low-frequency turbulence. Fig. 9b shows the normalized mean wind speed profile (U/U_{ref}), where, U_{ref} is the reference mean wind speed at the reference height (Z_{ref} = 10 m at full scale). Fig. 9a shows the turbulence intensity (I_u) at the MRH of each case after adding the missing low-frequency turbulence. And Fig. 9b shows the normalized mean wind speed profile (U/U_{ref}), where, U_{ref} is the reference mean wind speed at the reference height (Z_{ref} = 10 m at full scale).

The PTS method was developed and validated by Mooneghi et al. and Moravej [34,35]. And it has been widely adopted in the large-scale wind tunnel testing field [36]. More details about this process were provided in the previous test of elevated houses by Abdelfatah et al. [22]. The final local peak pressure coefficients are presented in the next section of this paper.

The area-averaged peak pressure coefficients ($C_{P,\ avg,\ peak}$) were calculated for each surface to show their variation with wall height (h) and stilt height (S_h). Applying a full range of wind directions (i.e., 0–360° with 3° increments) increases the confidence to develop a zoning scheme for the floor surface. In this regard, the $C_{P,\ avg,\ peak}$ values were calculated and are proposed in this paper. For different cladding floor areas, a comparison is done between $C_{P,\ avg,\ peak}$ obtained in the current study and the external pressure coefficients for a flat roof recommended by ASCE 7-16 (2016). The procedures for calculating $C_{P,\ avg,\ peak}$ are explained in detail by Abdelfatah et al. [22]. The following section presents the resulting pressure coefficients and wind forces for the tested cases. The effect of elevating the house on the airflow streamlines is

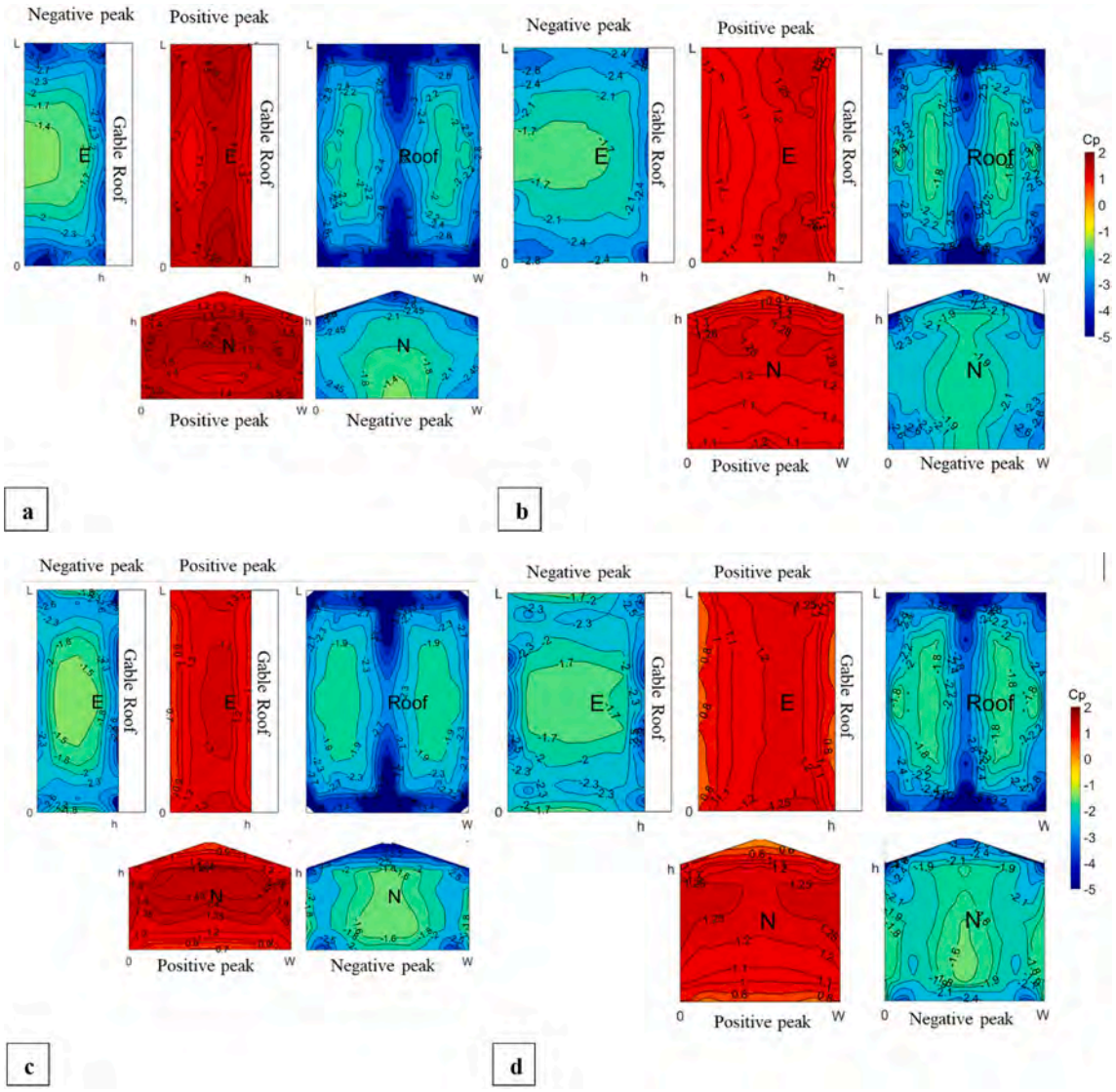

Fig. 11. Maximum and Minimum local peak pressure coefficients (C_{Ppeak}) among all wind directions (a) case 1S-0, (b) case 2S-0, (c) case 1S-104, and (d) case 2S-104.

examined. The wind effect on the floor surface is presented and compared with the roof surface wind loading results.

3. Results and discussion

Testing the gable roof model using different number of stories and stilt heights enabled the authors to perform a comparative study on the aerodynamics of elevated and on-ground house cases. In this section, the wind flow characteristics are visualized, and the resulting wind pressure effect is demonstrated as well. The eight tested models, as mentioned in Table 1, were numerically simulated using Computational Fluid Dynamics (CFD) to present the flow streamlines. This simulation contributes to understanding the building aerodynamics, the change in wind pressures along the model surfaces, and attempts to understand the damage modes observed in recent hurricanes.

Furthermore, the experimental test results are provided in this section, including area-averaged and peak pressure coefficients for all surfaces, including the floor surface. The wind forces were computed and compared to on-ground cases. Moreover, a floor zoning scheme and area-averaged peak pressure coefficients are proposed in this section. The proposed floor zoning and wind loading information is compared to these available for flat roof surfaces in ASCE 7-16 (2016). Finally, a set of design recommendations for elevated houses, including the floor surface, is proposed.

3.1. Aerodynamic flow simulation using CFD

The experimentally tested elevated house models were also modeled using Computational Fluid Dynamics (CFD) to visualize the wind flow around the building. The full-scale (prototype) size of the tested on-ground and elevated models were simulated using Reynolds-Averaged Navier-Stokes (RANS) equations. The RANS model was considered sufficiently accurate and computationally economic to provide guidance on mean wind loading [37,38]. Following the recommendations published by [39], the domain size was calculated using the total model height (H), as shown in Fig. A.1 in Appendix A in this article. The domain dimensions (85 m in length, 44 m in width, and 38 m in height) were sufficient to avoid excessive effects from domain walls. The computational domain was meshed into tetrahedral cells. Mesh sensitivity analysis was done using the 1S-43 case, between coarse mesh (~1.7 M

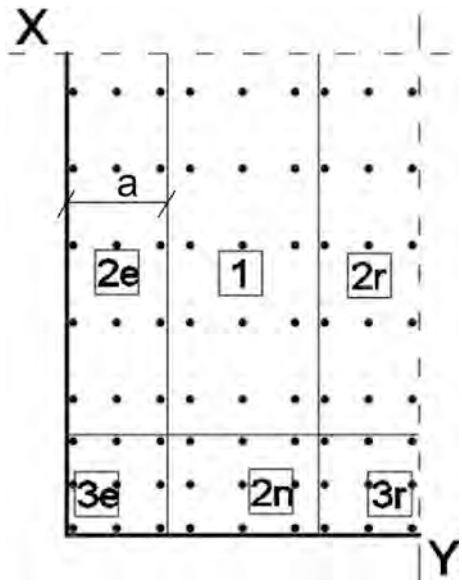

Fig. 12. Zone boundaries of the roof surface according to ASCE 7-16 and pressure taps' location for all the tested models.

cells), moderate mesh (~3.3 M cells), and fine mesh (~4.6 M cells). The moderate mesh showed good performance and agreement with the experimental results. However, to precisely simulate the flow separation, reattachment, and vortices, the fine mesh was chosen, as shown in Fig. A.2. For the large stilt cases, the number of mesh cells exceeded 5 million cells. The cell size near the model walls was H/48 and the rate of mesh size increase did not exceed 20%. Mesh refinements were applied around the stilts to precisely monitor the flow separation. At the vertical direction, the first cell height is around 3.2 mm to keep the dimensionless wall distance (Y +) in the range (30–300) to model the log-law layer [40]. In the literature, RANS (k-ε) and (k-ω) turbulent models showed a good performance and successfully simulated wind effects on low-rise gable roof buildings [26,41,42]. Where k is the turbulence kinetic energy, ε is the turbulence dissipation rate, and ω is the specific dissipation rate. The (k-ε) RNG turbulent model was chosen as it showed better performance [37,43]. In addition, after comparing the resulting C_{pmean} of (k-ε) and (k-ω) on the roof surface, the RNG (k-ε) agreement with WOW is more acceptable, especially in the high suction region, as shown in Fig. A.3.

The wind turbulence intensity (I_u) was defined using Equations (2 and 3), where C_μ is the turbulence model constant which was taken as 0.09 (Gorlé et al., 2009). The turbulence dissipation rate (ε) was calculated using Equation (4) as recommended by Richards et al. [44].

$$K(Z) = \frac{u^{*2}}{\sqrt{C_\mu}} \tag{2}$$

$$K(Z) = \frac{3(IuU)^2}{2} \tag{3}$$

$$\varepsilon(Z) = \frac{u^{*3}}{\kappa(Z+z)} \tag{4}$$

All the outer walls were defined as slip walls, and the ground surface was defined as a rough wall using the same roughness length as the prototype (z = 0.08 m). The roughness length was defined using input values; roughness height (Cs), roughness constant (Ks = 0.5), and calculated using Equation (5) [45].

$$C_s = \frac{9.793z}{K_s} \tag{5}$$

ANSYS FLUENT 19.0 commercial software was used. Naiver Stokes and continuity equations were solved using the control volume method. The computational equations were discretized using a second-order upwind scheme with standard pressure interpolation. The SIMPLE algorithm was used for pressure velocity coupling. To reduce computational errors or uncertainties, a range of 10^{-4}–10^{-7} was applied for the scaled residuals. The eight models were simulated for three wind directions (0°, 45°, and 90° angles). For validation purposes, the resulting mean pressure coefficients were compared for both numerical and experimental cases. Fig. A.4, in the appendix, shows the resulting mean pressure coefficients over the floor surface of the (1S-34) case for three wind directions. The comparison shows that the deviation between the numerical and experimental results is not exceeding 7%. More

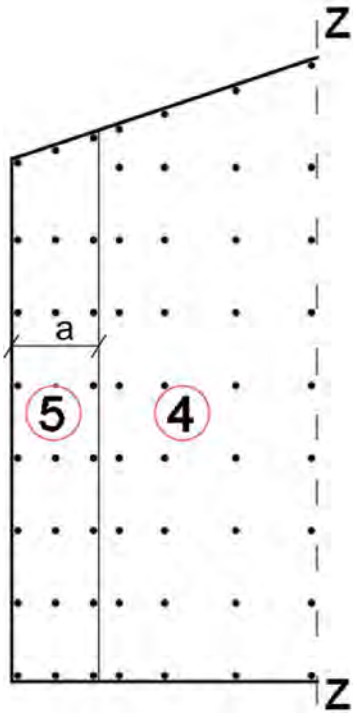

Fig. 13. Zone boundaries of the two-story wall surface according to ASCE 7-16 and pressure taps' location for all the tested models.

Table 2
Peak area averaged pressure coefficients ($C_{P,\ avg,\ peak}$) of the roof surface.

Test case / Zone	1S-0	1S-43	1S-73	1S-104	2S-0	2S-43	2S-73	2S-104
3e	−2.50	−2.42	−2.41	−2.26	−2.32	−2.09	−2.07	−2.12
3r	−3.02	−2.96	−3.02	−2.97	−2.78	−2.63	−2.67	−2.73
2e	−1.93	−1.78	−1.78	−1.72	−1.85	−1.65	−1.74	−1.68
2r	−2.40	−2.34	−2.23	−2.14	−1.97	−2.00	−1.85	−1.91
2n	−2.46	−2.30	−2.33	−2.26	−2.08	−2.06	−1.94	−2.00
1	−1.81	−1.72	−1.72	−1.68	−1.81	−1.63	−1.58	−1.63

Table 3
Negative $C_{P,\ avg,\ peak}$ values on walls of each stilt model.

Test case	*1S-0*	*1S-43*	*1S-73*	*1S-104*	*2S-0*	*2S-43*	*2S-73*	*2S-104*
Zone name	*Peak negative pressure coefficient ($C_{P,\ avg,\ peak}$)*							
4	−1.76	−1.73	−1.50	−1.48	−1.72	−1.57	−1.50	−1.56
5	−2.22	−1.93	−1.95	−1.88	−1.84	−1.64	−1.55	−1.64

Table 4
Positive $C_{P,\ avg,\ peak}$ values on walls of each stilt model.

Test case	*1S-0*	*1S-43*	*1S-73*	*1S-104*	*2S-0*	*2S-43*	*2S-73*	*2S-104*
Zone name	*Peak positive pressure coefficient ($C_{P,\ avg,\ peak}$)*							
4	1.24	1.03	1.01	0.98	0.97	0.86	0.81	0.83
5	1.25	1.08	1.07	1.04	1.00	0.91	0.85	0.92

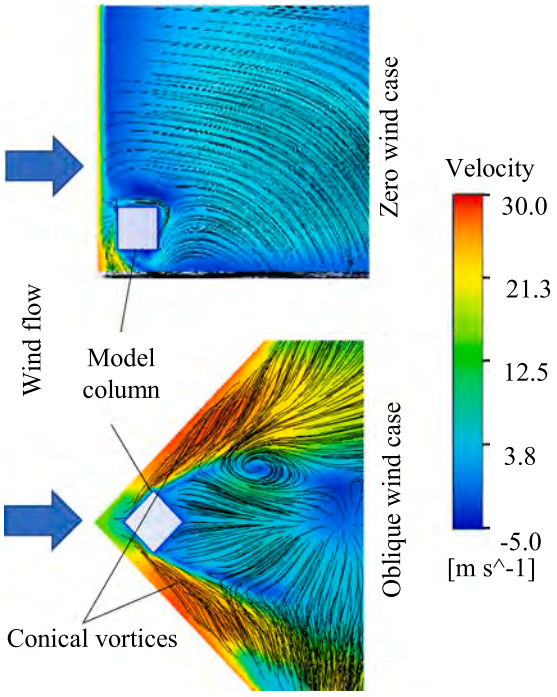

Fig. 14. A plan view of the 3D streamlines around the model stilt of 1S-43 case using CFD.

comparisons were also published by Abdelfatah et al. [46].

Wind flow streamlines help to understand the flow characteristics and the consequent wind loads. Fig. 10a shows the flow streamlines of various cases under 0° wind direction. The plot sections were taken along the ridgeline (mid-span B, as mentioned in Fig. 4). The effect of house elevation can be seen by comparing the 1S-0 and 1S-104 cases. The stagnation point is located at a higher level on the windward wall as the model elevation increases. This causes differences in the pressure distribution on the windward wall. The air circulation in the structure wake moves slightly down in the elevated case (1S-104) under 0° wind direction and a separated flow forms on the floor surface. And, in the case of 90° wind direction, the wake moves down until it merges with the separated flow formed below the floor, as shown in Fig. 10b in the case 1S-104. These changes in wake and flow separation zones result in higher wall suctions than that for the on-ground case. These findings agree with the observations discussed by Amini and Memari [26]. Under 0° wind direction, the flow separation formed above the model roof is larger in the elevated case (1S-104). Evidently, this is attributed to the roof height since a similar separation zone size was also observed in the two-story on-ground case (2S-0). In Fig. 10a, the comparison between 2S and 0 and 1S-43 shows two different aerodynamics with the same mean roof height from the ground. Above the model roof, the separation zone is similar in the two cases.

For various elevated cases, the floor surface is differently affected by wind. A vortex was formed just below the floor surface in the smaller elevated case, Fig. 10a (1S-43), causing local high suction. However, in the large stilt case (1S-104), the vortex formed away from the building, and the flow separation on the floor surface was enlarged resulting in a less concentrated suction. In Fig. 10b, the vortex formed, under 90° wind direction, is more critical and causes higher suction on the floor. The most important observation is the wind speed increase beneath the building floor. This observation justifies the reoccurring damages observed for the floor in elevated houses during extreme wind events. For instance, in the lower elevated case (1S-43), Fig. 10a shows that the velocity, at the marked locations 0.75 m above the ground level, increases from 12.3 m/s near the inlet and reaches 22.5 m/s (80% increase) below the model. In the higher elevated case, Fig. 10a (1S-104), the velocity below the model at the marked location reaches 17.2 m/s (39% increase). The velocity increase beneath the floor surface is more critical in the two-story case due to the larger blocked area of the two-story walls, as shown in Fig. 10b. The velocity reaches 23.5 m/s (91% increase) and 25.2 m/s (104% increase) in the cases 1S-104 and 2S-43, respectively.

3.2. Peak pressure coefficients on roof and walls

The above discussion on the flow streamlines provides some insights into changes in the local peak pressure coefficients calculated using the 3-s gust wind speed at the model MRH (C_{Ppeak}). The change in the C_{Ppeak} distribution on the wall surfaces can be noticed by comparing on-ground and elevated cases. For instance, a reduction of C_{Ppeak} positive values and an increase in C_{Ppeak} negative values occur at the lower zone of the elevated model walls compared to their on-ground counterparts. By comparing Fig. 11a with Fig. 11c, the C_{Ppeak} positive values decreased by 60% at the lower region, while a blue strip of high negative C_{Ppeak} values appears at the lower end of the walls of the elevated case (1S-104). This is observed as well for the two-story elevated cases (see Fig. 11d). On the other hand, the roof surface pressure coefficients did not exhibit significant differences between the tested cases. Roof C_{Ppeak} negative values are higher in the on-ground one-story case and slightly decrease as the elevation increases. These observations agree with the previously reported results by the authors on a one-story elevated house [22] and [26].

The peak area-averaged wind pressure coefficients ($C_{P,\ avg,\ peak}$) were analyzed to estimate wind loading on Components and Cladding zones. Those values were calculated for each stilt case using the corresponding 3-s wind speed at the mean roof height (MRH). The procedure of calculating $C_{P,\ avg,\ peak}$ was done by following the recommendations provided by the ASCE 7-16 and explained in detail by Abdelfatah et al. [22]. Fig. 12 illustrates the roof zone division for the tested models according to the ASCE 7-16. The figure also shows the distribution of pressure taps located in each zone. The dimension "a," which defines the size of each zone, was taken to be 0.9 m (full-scale) (18 cm model-scale).

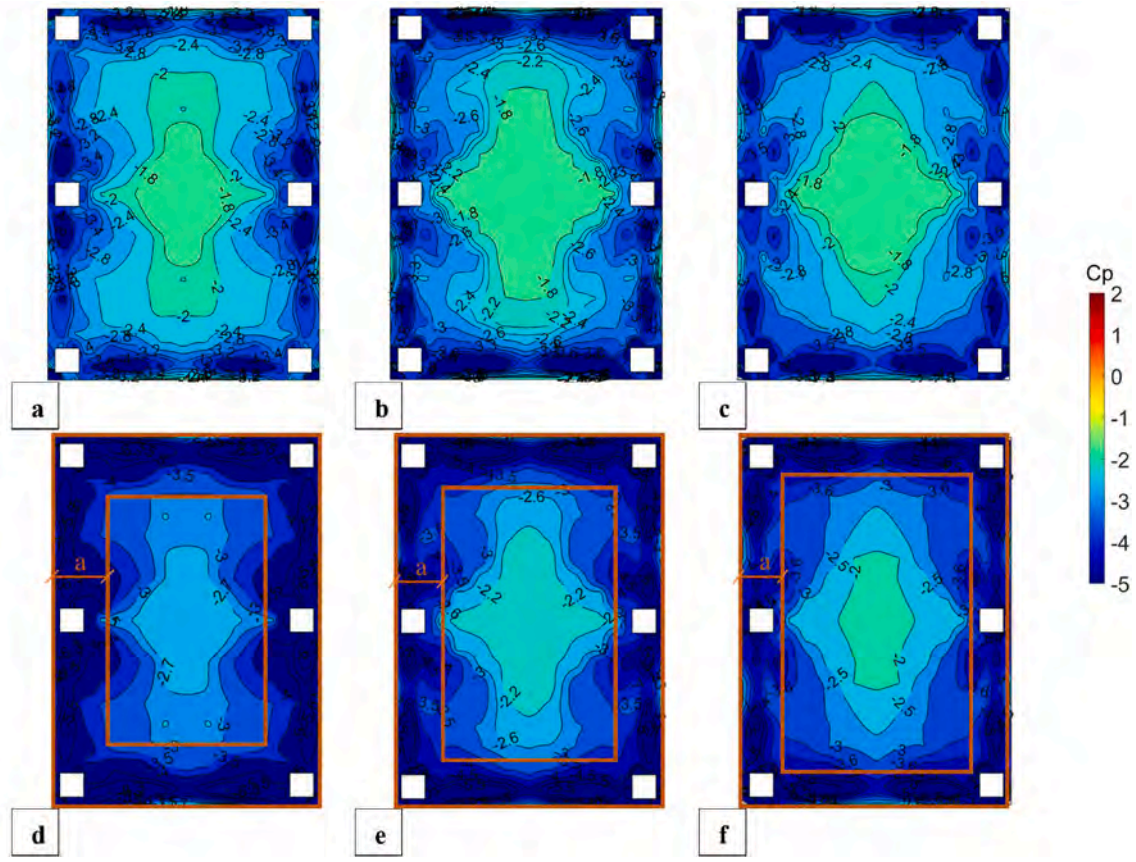

Fig. 15. Minimum C_{Ppeak} contours on the floor surface among all wind directions (a) case 1S-43 using reference velocity at MRH, (b) case 1S-73 using reference velocity at MRH, (c) case 1S-104 using reference velocity at MRH, (d) case 1S-43 using reference velocity at floor level, (e) case 1S-73 using reference velocity at floor level, and (f) case 1S-104 using reference velocity at floor level.

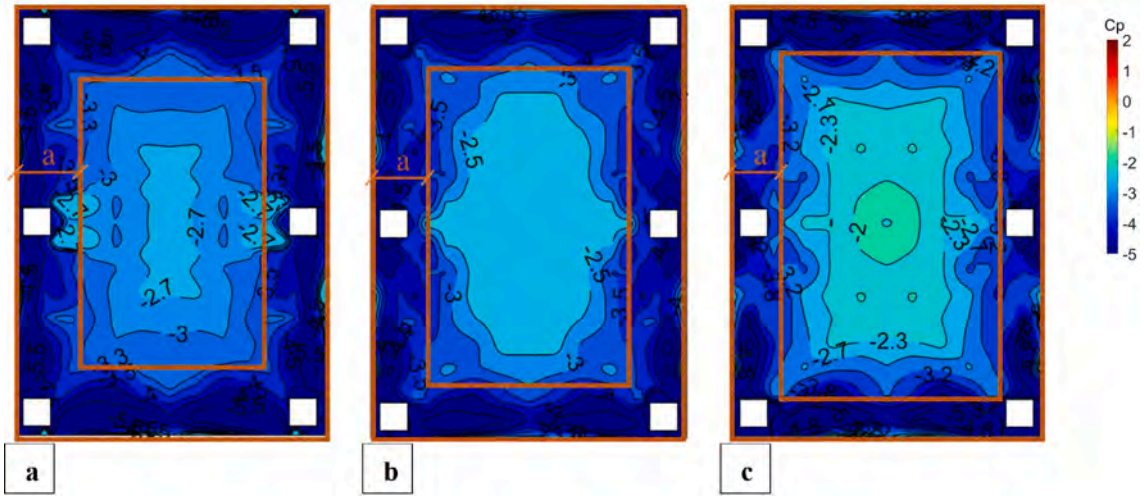

Fig. 16. Minimum C_{Ppeak} contours on the floor surface among all wind directions using reference velocity at floor level (a) case 2S-43, (b) case 2S-73, (c) case 2S-104.

For every possible tributary area, the recorded pressure time histories were averaged and normalized to obtain a time history of area-averaged wind pressure coefficients. The PTS method was applied to the resulting time history to calculate the $C_{P,\ avg,\ peak}$.

Table 2 summarizes the resulting $C_{P,\ avg,\ peak}$ for the roof zones obtained for the eight tested models while considering the worst case of all tested wind directions and tributary area 0.9 m^2. The $C_{P,\ avg,\ peak}$ values look consistent with no significant variations. They exhibit a slight tendency to decrease as the stilt height increases. The one-story cases exhibit higher $C_{P,\ avg,\ peak}$ values range between 10% and 20% compared to two-story cases. Compared to the 1S-0 case, the $C_{P,\ avg,\ peak}$ values of the one-story elevated cases are 5% lower at the middle zone and 10%

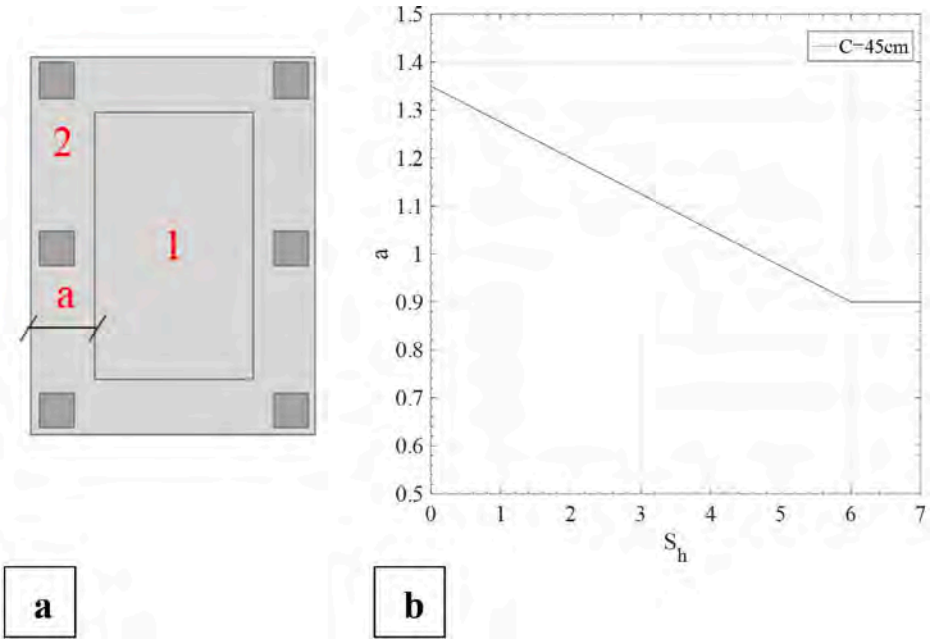

Fig. 17. Proposed zone boundaries of the floor surface; (a) zone labeling, and (b) zone width (a) relation with the stilt height (S_h).

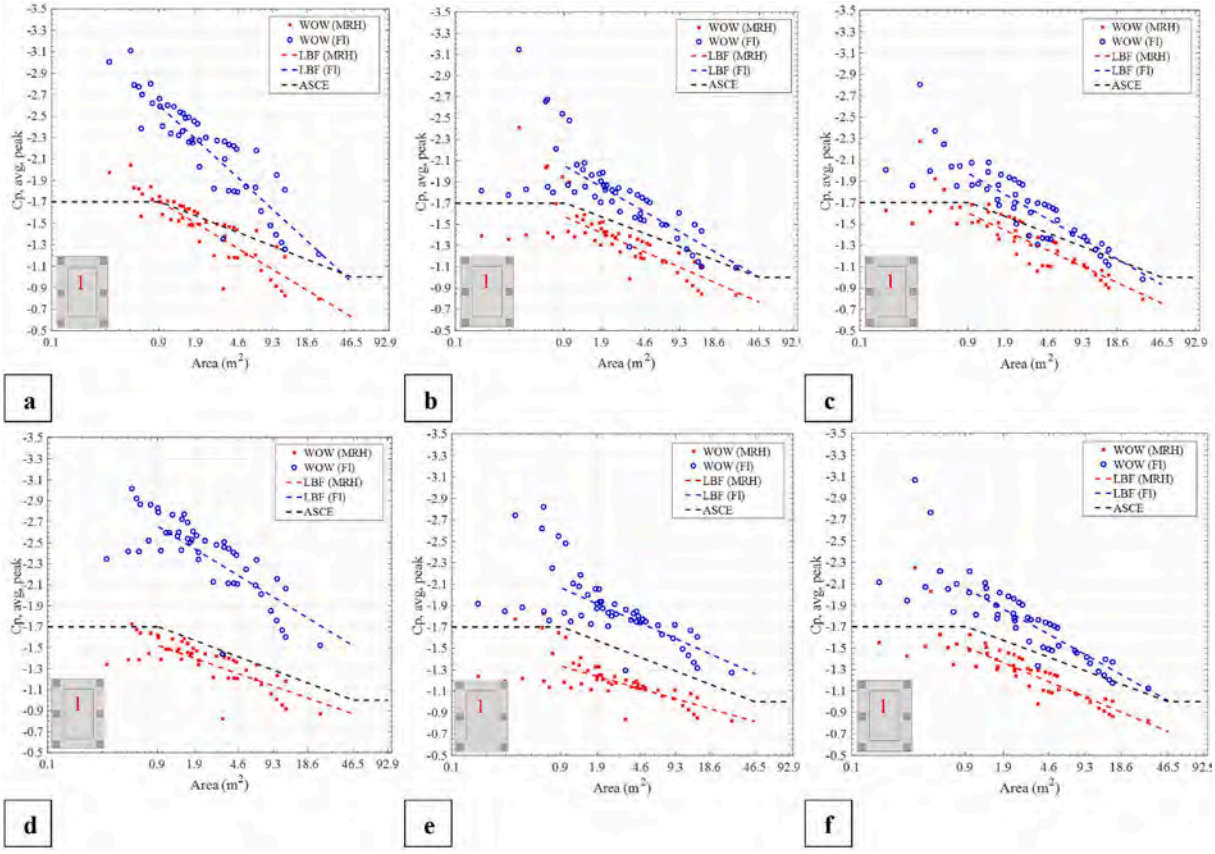

Fig. 18. $C_{P,\ avg,\ peak}$ for the middle zone 1 for different effective tributary areas (a) case 1S-43, (b) case 1S-73, (c) case 1S-104, (d) case 2S-43, (e) case 2S-73, and (f) case 2S-104.

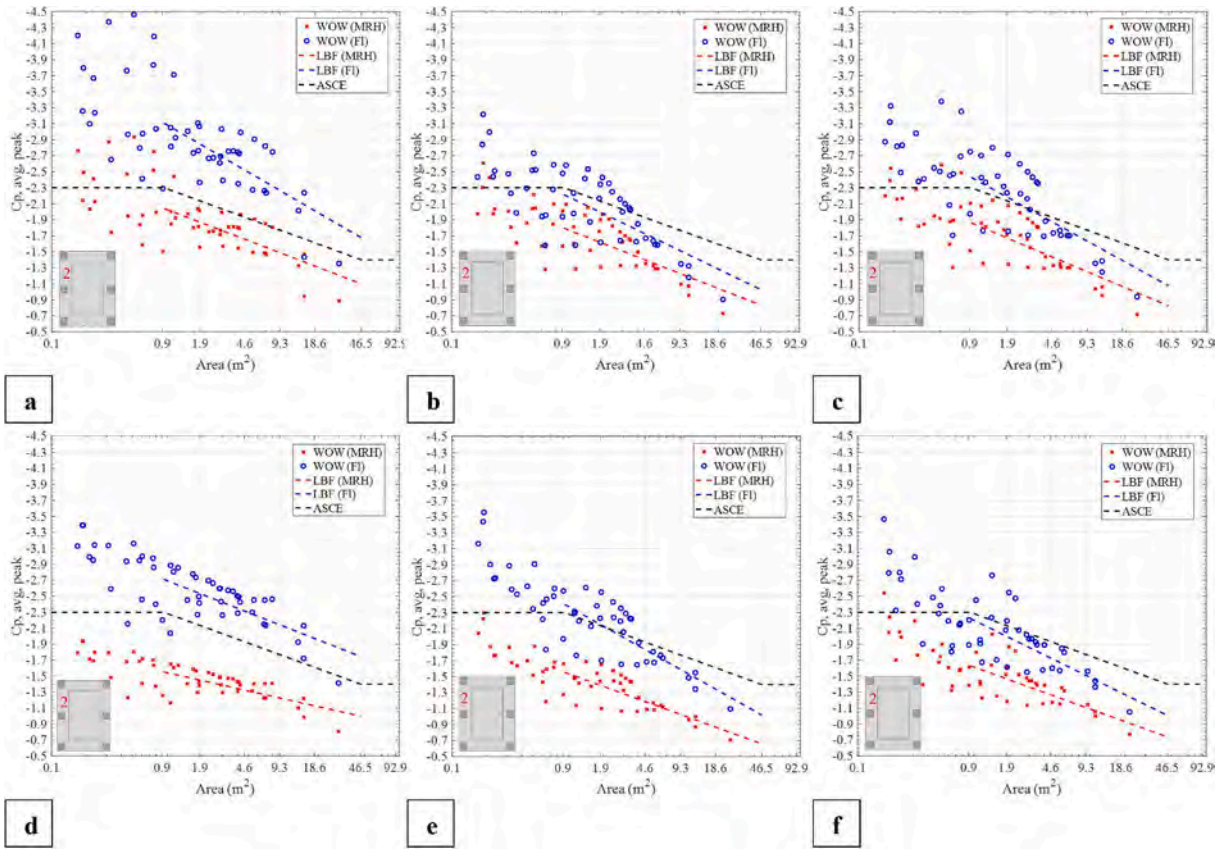

Fig. 19. $C_{P,\ avg,\ peak}$ for the edge zone 2 for different effective tributary areas: (a) case 1S-43, (b) case 1S-73, (c) case 1S-104, (d) case 2S-43, (e) case 2S-73, and (f) case 2S-104.

Table 5
Negative $C_{P,\ avg,\ mean}$ values on the floor of all the tested cases.

No. of stories	*One-Story*			*Two-Story*		
Stilt case	*1S-43*	*1S-73*	*1S-104*	*2S-43*	*2S-73*	*2S-104*
WOW (Fl)	−0.98	−0.78	−0.73	−1.1	−0.92	−0.8

lower at the edge zones. While for the 2S-0 case, the $C_{P,\ avg,\ peak}$ values of the elevated cases are 12% lower at the middle zone 7% lower at the edge zones. Using the mean roof height wind speed as a reference implies an increase in the global and local uplift wind forces on the roof as the mean roof height increases.

The same procedures were applied on the wall surfaces. Fig. 13 clarifies the zone boundaries for the walls according to ASCE 7-16. Similarly, zone 5 width (a), was taken to be 0.9 m (full-scale) (18 cm model-scale). Tables 3 and 4 show the negative and positive $C_{P,\ avg,\ peak}$

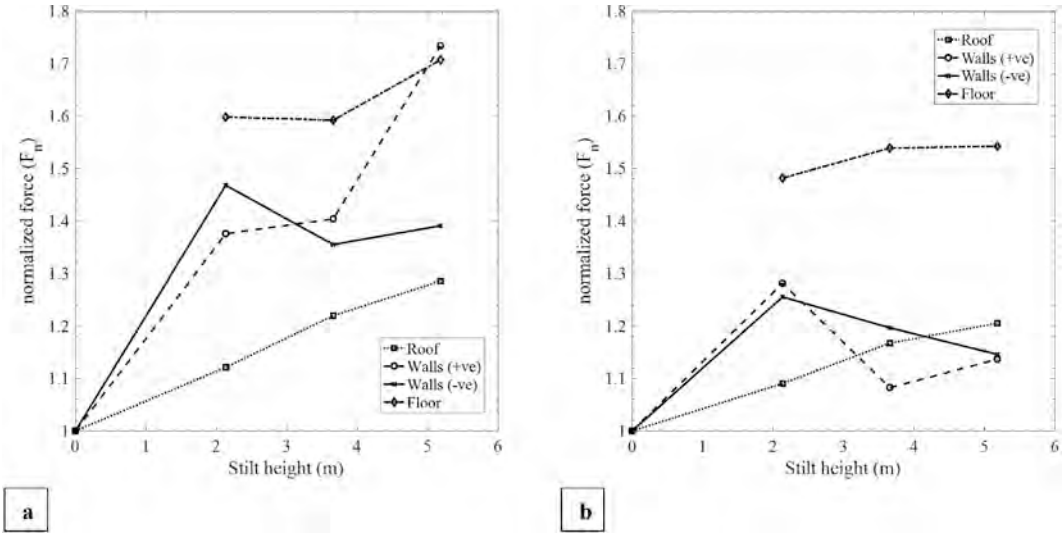

Fig. 20. Normalized mean wind forces on each surface (a)one-story, and (b)two-story.

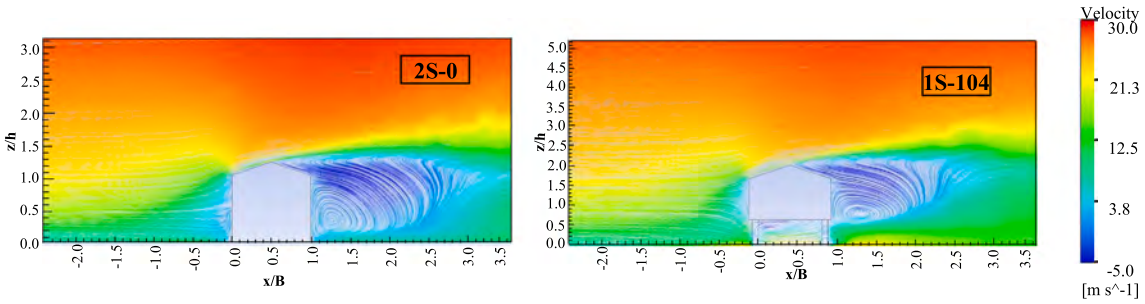

Fig. 21. Streamlines of the two compared on-ground and elevated cases.

values corresponding to tributary area 0.9 m^2 (full scale), representing the envelope of all wind directions. The table shows that both positive and negative averaged coefficients are more critical in the on-ground cases. The positive $C_{P,\ avg,\ peak}$ values in the one-story and two-story elevated cases are lower by 20% and 15%, respectively, compared to their on-ground counterparts. Additionally, the two-story cases $C_{P,\ avg,\ peak}$ values are 20% lower than one-story cases. The negative $C_{P,\ avg,\ peak}$ is not noticeably affected by the elevation in case 1S-43 compared to the on-ground replica. However, in the taller stilt cases (1S-73) and (1S-104) $C_{P,\ avg,\ peak}$ values are around 15% lower than the on-ground case. This increase possibly is due to the use of larger reference wind velocity for taller buildings.

The presented results indicate that a simple conservative approach would be to use the on-ground pressure coefficients to design roofs and walls of elevated cases. This agrees with the recommendations provided by the Australian and New Zealand wind loading standard [28], which provides the same pressure coefficient value for an elevated house's walls as for the on-ground case. The AS/NZS 1170.2 standard provides averaged pressure coefficient values (0.8 & −0.6) for the floor underside regardless of its dimensions [28]. No advice is currently available in the ASCE 7-16 standard on elevated buildings.

3.3. Floor surface zoning scheme and proposed pressure coefficients

In this section, floor local peak coefficients are provided, and a scheme for pressure distribution zoning is proposed. Based on the proposed zoning scheme, the area-averaged pressure coefficients for different effective areas are presented as well. In addition, the analyzed data from the current wind tests are compared with available design provisions for flat roof surfaces of low-rise buildings in ASCE 7-16 (2016).

3.3.1. Local peak pressure coefficients on the floor surface

The velocity streamlines shown in Fig. 14 reveal the flow separation at the edge of the floor surface in both wind directions 0° and 45°. In the 0° direction case, the streamlines show the occurrence of flow separation at the column edges and air circulation taking place at the floor corner. However, no pronounced vortex shape was found as in the 45° case. The noticed flow separation justifies the high local suction at the edges of the floor surface, as shown in Fig. A.4 in the appendix. It worth mentioning that, in case of wind acting in the oblique direction, higher suction region appears around the stilts. As shown in Fig. 14, the plan view of the flow streamlines below the model floor surface shows conical vortices formed in case of oblique wind direction with higher wind speeds compared to the 0° wind case. These vortices are the main reason for the suction regions occurring along the sides of the stilts.

Fig. 15a-c show the peak local pressure coefficient values among all wind directions for the one-story elevated cases. The pressure coefficients were calculated by taking the reference velocity at the MRH. The figure shows high suction regions observed along the floor edges. However, using the mean roof height as a reference height to calculate the pressure coefficient on the floor was not optimum to present the effect of changing the model stilt height. This is particularly important when looking at the effect of one-story vs two-story cases. By comparing with Fig. 15d-f, which present the normalized pressures using floor height velocity as a reference, Fig. 15a-c show smaller coefficients that are not consistent with the flow streamline observations that indicate a lower suction on the floor as the stilt height increases. In addition, Fig. 15a-c indicate slight differences in the pressure coefficients without a noticeable trend. In contrast, Fig. 15d-f show a more consistent trend in the resulting pressure coefficients on the floor. For this reason, C_{Ppeak} normalized using reference wind velocity at the floor surface will be used to determine the zoning scheme for the floor surface. This also helps in evaluating the differences between one-story and two-story cases. More discussion on these observations is provided in the next section.

3.3.2. Floor zoning scheme and area-averaged pressure coefficients

Fig. 15 d-f and Fig. 16 a-c show the C_{Ppeak} contour plot for one-story and two-story elevated cases. As stated in the previous section, the reference velocity is taken at the floor level. A slight reduction in the width of the high suction region occurs as the stilt height increases for both one-story and two-story cases. However, the one-story case exhibits higher pressure coefficient values compared to the two-story-one. In the smallest stilt case (1S-43), the C_{Ppeak} ranges between −6.3 and −3.5 along the edges and reaches −2.7 at the middle region. In case 2S-43, the C_{Ppeak} range at the edge is between −5.5 and −3.3. The C_{Ppeak} values, normalized using dynamic pressure at the floor level, were used to obtain a zoning scheme for the floor surface. Abdelfatah et al. suggested dividing the floor surface into three zones: a column zone, an edge zone, and a middle zone [22]. However, adding intermediate columns in this study caused an additional suction along the floor edge. Therefore, it is recommended to merge the edge and column zones into one zone. Consequently, the floor surface is divided into two zones. More investigations are needed for different column patterns.

Fig. 17a demonstrates the proposed zones for similar floor surfaces: middle zone (1), and edge zone (2). This zoning scheme is similar to the one provided by the ASCE 7-16 standard for a flat roof. For each zone, the area average pressure coefficients ($C_{P,\ avg,\ peak}$) were calculated for different tributary areas and are plotted as shown in Figs. 18 and 19. The width of zone 2 is a variable named "a" which was empirically estimated using Equation (6). This equation is recommended to be used under two conditions: (1) the column width "c" shall not be less than S_h/10 and, (2) the zone width "a" shall not be less than 2c. As the relationship between the stilt height and zone width "a" is consistent in the one-story and two-story cases, the paper suggests using the same equation for different numbers of stories.

$$a = 3c - \frac{3S_h}{40} \quad (6)$$

where S_h is the floor height, and c is the column width.

For the current case of study, the column size was fixed (0.45 m in full scale), the relation between the zone width (a) and the stilt height (S_h) is drawn (Fig. 17b). The graph reveals the inverse relation between the two variables, for any given (*c*). The decrease of the zone width stops when it reaches twice the stilt width (0.9 m in full scale), and it remains constant after that.

Fig. 18 shows the variation of $C_{P,\ avg,\ peak}$ with the corresponding effective tributary areas for zone 1. The plots show the resulting $C_{P,\ avg,\ peak}$ normalized using dynamic velocity at (1) the mean roof height (WOW (MRH)) and at (2) the Floor level (WOW (Fl)). The plots also include the logarithmic relation between the external pressure coefficient and cladding effective area on a flat roof surface according to ASCE 7-16. To easily compare the floor pressure coefficients with these recommended for a flat roof provided by ASCE 7-16, the Logarithmic best fit (LBF) line was computed for the WOW data. The figure facilitates the evaluation of wind loading using different velocity reference heights. For the one-story cases, Fig. 18a-c, the $C_{P,\ avg,\ peak}$ normalized using MRH velocity are close or lower than the ASCE external pressure coefficients for a flat roof. This is observed in the two-story cases too (Fig. 18d-f). This indicates that using the pressure coefficients of a flat roof surface to calculate wind forces on elevated building floor surface is conservative if the reference wind velocity is taken to be at the mean roof height. However, using the wind velocity at the floor surface, the recommended pressure coefficient for zone 1 ranges between −2.7 and −1.5 for tributary areas ranging between 0.9 m^2 and 46.5 m^2(full scale), respectively.

For the edge zone (2), the same observations are noticed in Fig. 19 a-f. The ASCE $C_{P,\ avg,\ peak}$ values for a flat roof are much conservative compared to the WOW (MRH) values. Therefore, the ASCE values can be conservatively used to calculate vertical forces on the floor surface while using the reference wind velocity at the mean roof height. Otherwise, the $C_{P,\ avg,\ peak}$ on the floor surface can be calculated using a logarithmic relation of $C_{P,\ avg,\ peak}$ ranging between −3.1 and −1.7. The ASCE 7-16 standard recommends using external pressure coefficients −0.9 and −0.6 for the edge zone and the middle zone of the elevated tanks. From the shown results, it is clear that both values are not applicable to be used in case of elevated houses.

In the current study, the mean pressure coefficients ($C_{P,\ mean}$) were also averaged over the whole floor surface to get $C_{P,avg,\ mean}$. Because only the quarter was instrumented, the mean coefficients are used as it could be derived using the model symmetry. Table 5 lists the resulting $C_{P,avg,\ mean}$ values on the floor surface for the critical case 90° wind direction. For the current tested cases, the external pressure coefficients were calculated using the AS/NZS 1170.2 standard. This aims to compare the recommended external coefficients by AS/NZS 1170.2 standard against real conditions. The recommended negative external pressure coefficient over the floor surface is −0.6, which is 8–45% lower than WOW (Fl) $C_{P,\ avg,\ mean}$ value. It worth mentioning that the pressure coefficients provided by the standard should cover peak values as well. Therefore, further investigation should be done to provide external pressure coefficients for the floor surface.

The aim behind this was to compare the results with the AS/NZS 1170.2 standard.

More studies are required on different configurations of elevated houses with various distributions of stilts to validate and codify external pressure coefficients for the floor surface. Until then, the authors recommend using the wind velocity at the building roof height to calculate the wind loads on the floor surface.

3.4. Mean wind forces on the model surfaces and the expected effects

It is of interest to investigate the total wind forces acting on the building surfaces to provide an insight into the overturning moment and base shears acting on the building. For each surface of the tested models, the mean wind force was calculated for every wind direction and normalized to the corresponding wind force for the counterpart on-ground case. Only for the floor surface, the wind force was normalized to the roof wind force multiplied by −1. Fig. 20a-b show the variation of the normalized wind forces (F_n) with the stilt height (in full scale) for all surfaces. In general, the figure shows that elevated buildings experience higher forces compared to these imposed on an on-ground counterpart. For the roof surface, the plot is for the critical wind direction (60°) which causes the highest suction. The plots show a gradual increase in the roof suction force till it reaches 29% and 21% in the one-story case and two-story case, respectively. However, for the windward wall positive force and under the critical wind direction (0°), there was no certain trend; the increase is significant in the one-story case, unlike the two-story case. Fig. 20a-b also show that the sidewalls' maximum suction force, for the wind direction (0°), occurs in the shortest stilt cases (1S-43) and (2S-43).

For the floor, the critical wind case was found to be 90°. Fig. 20 reveals that the vertical force, acting on the floor downward, is always larger than the roof suction force. For the one-story case, the increase is 60% for the 1S-43 and 1S-73 cases and 70% for the 1S-104 case. On the other hand, in the two-story case, the increase is 48% for the 2S-43 case and around 54% for the 2S-73 and 2S-104 cases. The percentage is lower in the two-story case because the force acting on the roof is more significant due to the increase in the wind speed at larger heights. In conclusion, the stilt height significantly affects the resulting total vertical, shear force, and overturning moment acting on the house foundations.

To further investigate the effect of the air gap underneath the elevated model while eliminating the effect of the MRH, a comparison is conducted between the mean forces calculated for the 1S-43 and 2S-0 cases. These two cases are chosen as they have the same MRH, around 6 m (full-scale). As shown in Fig. 21, the airflow over the model roof in the two cases looks similar. However, the presence of air gap significantly affects the streamlines, as illustrated in section 3.1.

The resulting mean forces show that the roof forces on the two models are approximately equal. For wind acting parallel to the roof ridge, the wall surfaces experience 30% lower suction force and 22% lower pressure force in the elevated case (1S-43). This is due to the reduction of the area affected by wind. Finally, the floor surface added a new vertical force, which is 19% higher than the force acting on the roof in case of wind acting perpendicular to the model ridge. Such force will reduce the overall tension on the building foundations.

4. Conclusion

An experimental investigation of wind effects on elevated houses complemented by numerical simulation using Computational Fluid Dynamics (CFD) methods was conducted. First, a commonly used coastal house configuration was tested using large-scale models at the Wall of Wind (WOW) Experimental Facility under different wind directions. This study considered two building types: (1) One-story and (2) Two-story gable roof models. For each building type, four cases were considered: (a) an on-ground house, (b) at 2.15 m elevation, (c) at 3.65 m elevation, (d) at 5.2 m elevation. Also, the wind-structure interaction for the tested models was computationally simulated using CFD RANS simulations to study the wind flow and assess elevated buildings' aerodynamic behavior compared to an on-ground building.

Local peak pressure coefficients (C_{Ppeak}), calculated using the experimental pressure time histories, were used to present contour plots

along each surface for the on-ground and elevated building cases. Compared to their on-ground counterpart, the following observations were found for the elevated buildings: (1) No significant change was observed in C_{Ppeak} values of the roof surface for the elevated cases; (2) The wall surfaces of the elevated cases experienced lower positive and higher negative C_{Ppeak} at the lower edge due to the flow separation; (3) High suction regions along the floor underside edges and around the stilts were observed.

For the floor underside surface, the flow streamlines and the resulting pressure coefficients showed that the vortices formed in shorter stilts cases more suction force than taller stilts cases. From the flow streamlines and the resulting pressure distribution, the study concluded that the higher suction along the edges is caused mainly due to wind acting perpendicular to the roof ridge. However, the wind acting at oblique directions is responsible for the high suction around the stilts. An increase in the wind velocity was noticed, especially in the small stilt cases, beneath the model floor. This wind speed increase is believed to be responsible for the damage of house attachments and stairs that occurred in the past hurricanes.

From the variation of the peak pressure coefficient on the floor underside surface, a zoning scheme was proposed. The proposed zoning scheme adopts an empirical equation that incorporates the column's width and stilt height to calculate the width of the high suction edge zone. Based on the suggested zoning, the area-averaged pressure coefficients were calculated for the floor underside and compared to flat roof external coefficients available in the ASCE 7-16 standard. This comparison showed the applicability of using the pressure coefficients provided by ASCE 7-16 for a flat roof to calculate wind forces on the floor underside surface of an elevated house where the reference wind velocity is taken at the mean roof height of the elevated house building. Otherwise, higher pressure coefficients should be used if the floor level is considered at the reference height.

The experimental results show a considerable increase in the overall (global) uplift force on the roof surface and on the floor underside, especially in the one-story elevated cases, as the stilt height increases. This floor suction, acting downward, is larger than the force acting upward on the roof surface. However, by investigating two models with the same mean roof height while one is on-ground and the other is an elevated model, a reduction was found in the suction and pressure forces.

As with any experimental investigation, the current results were obtained on a limited number of building configurations. It would be useful in the future to examine other building shapes and stilt arrangements as well as the effects of partially blocking the underneath of the building.

CRediT authorship contribution statement

Nourhan Abdelfatah: Conceptualization, Methodology, Software, Validation, Formal analysis, Investigation, Data curation, Writing – original draft, Visualization. **Amal Elawady:** Conceptualization, Methodology, Formal analysis, Investigation, Writing – review & editing, Data curation, Visualization, Project administration, Funding acquisition, Supervision. **Peter Irwin:** Conceptualization, Methodology, Formal analysis, Investigation, Data curation, Visualization, Writing – review & editing, Resources, Supervision. **Arindam Gan Chowdhury:** Conceptualization, Methodology, Software, Formal analysis, Investigation, Resources, Writing – review & editing, Project administration, Funding acquisition, Supervision.

Declaration of Competing Interest

The authors declare that they have no known competing financial interests or personal relationships that could have appeared to influence the work reported in this paper.

Acknowledgments

All the experimental wind tests were conducted at the Wall of Wind (WOW) Experimental Facility (EF) and supported by the National Science Foundation (NSF), United States (Award# 1520853 & 2037899). The authors gratefully acknowledge the cooperation of the WOW staff members. The authors sincerely acknowledge the financial contribution of The State of Florida Division of Emergency Management (FLDEM). The authors acknowledge the financial support of Florida International University Graduate School (UGS) to the doctoral student Nourhan Abdelfatah through the Dissertation Year Fellowship (DYF). The opinions of the authors expressed herein do not necessarily state or reflect those of the sponsors.

Appendix A

In this appendix, more information about the CFD model of elevated buildings. The domain size empirical values are shown in Fig. A.1, which agrees with the provided recommendations in the literature [47]. Fig. A.2 shows the domain mesh of the 1S-43 case. The WOW atmospheric boundary layer was precisely simulated by using fine layers near the ground. The mesh resolution near the model is increased to better resolve the finer details of the flow in critical regions.

A comparison study was done to choose the turbulent model. Fig. A.3 shows the resulting C_{pmean} along the ridgeline of the roof surface (1S-43 case) under 0° wind direction, for two different turbulent models, (k-ε) RNG and (k-ω) SST [48]. Where k is the turbulence kinetic energy, ε is the turbulence dissipation rate, and ω is the specific dissipation rate. SST stands for the shear stress transport formulation, which switches the model to (k-ε) behavior. Comparing both results with WOW C_{pmean} shows a better agreement using (k-ε) RNG turbulent model.

Fig. A.4 shows the resulting C_{pmean} for the floor surface of both WOW and CFD. The plots highlight the agreement between the two cases. In the zero-wind angle, the C_{pmean} gradient is similar for both plots (CFD and WOW); the high suction (-0.84) occurs at the windward region and gradually drops to be −0.15 at the leeward region. Higher local suction (-0.92) occurs near the columns. For the 45° and 90° wind angles, the high and low suction regions agree well in both cases. However, the WOW plots show 5% higher C_{pmean} than CFD near the columns.

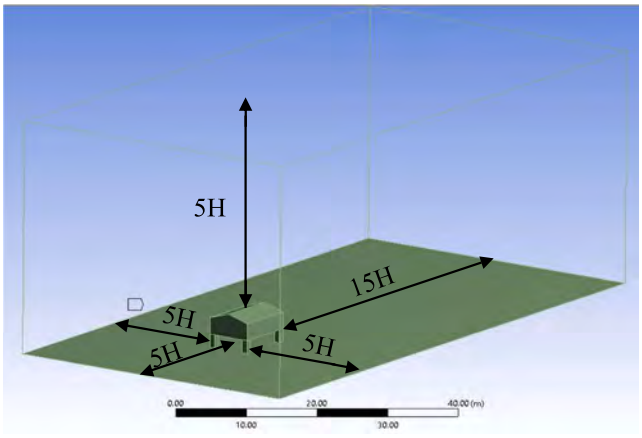

Fig. A1. The figure is taken from Ansys fluent software to show the computational domain dimensions.

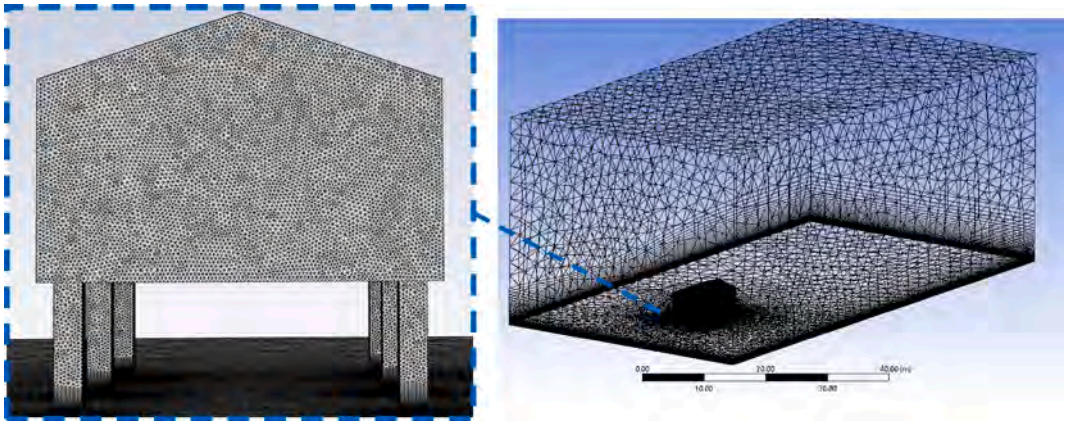

Fig. A2. 3D and frontal view of the simulated 1S-43 CFD model mesh using Ansys fluent.

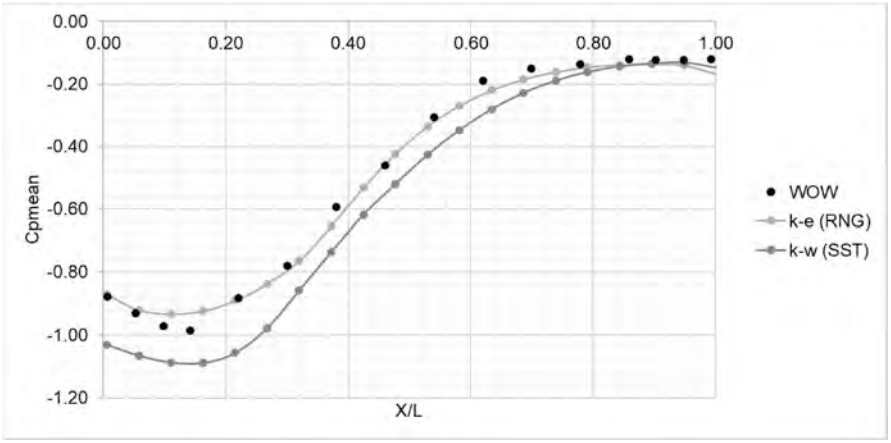

Fig. A3. C_{pmean} comparison (k-ε) RNG and (k-ω) SST with WOW for the roof surface of 1S-43 case under 0° wind direction.

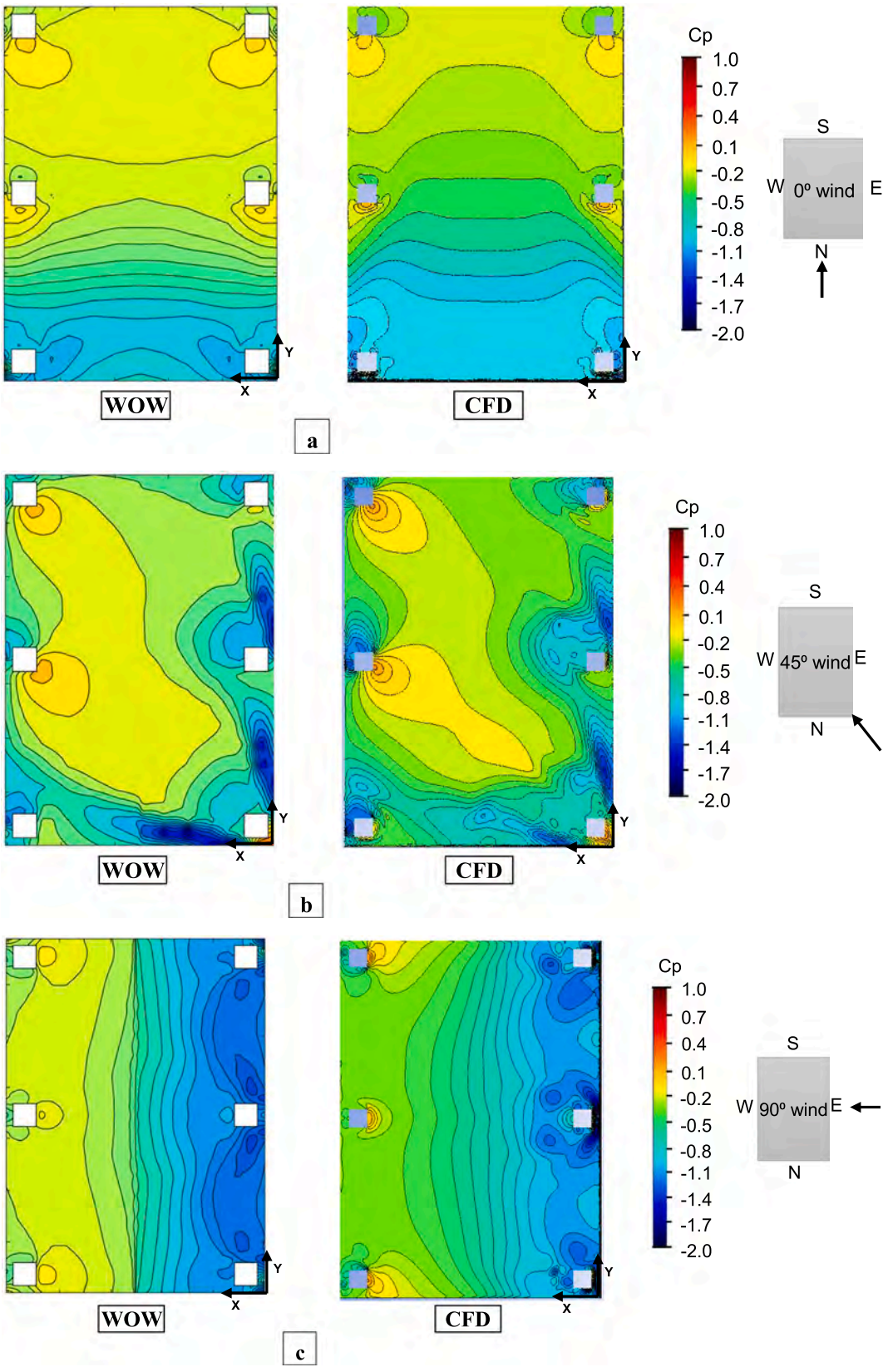

Fig. A4. C_{pmean} comparison between WOW and CFD for 1S-43 case (a) 0° wind direction, (b) 45° wind direction, and (c) 90° wind direction.

References

[1] NSF. The National Science Foundation (NSF), Network, and Structural Extreme Events Reconnaissance (StEER); 2019. https://web.fulcrumapp.com/apps/be73ae35-9ca8-43dd-aaff-469cc348ffed.

[2] UN. Engaging People to Protect the Planet; 2017. https://www.un.org/sustainabledevelopment/wp-content/uploads/2017/05/Ocean-fact-sheet-package.pdf.

[3] Hinrichsen D. Coasts in Crisis. Issues Sci Technol 1996;12:39–47.

[4] NOAA. Minor Modification to Saffir-Simpson Hurricane Wind Scale for the 2012 Hurricane Season; 2012. https://www.nhc.noaa.gov/pdf/sshws_2012rev.pdf.
[5] Amini M, Memari AM. Review of Literature on Performance of Coastal Residential Buildings under Hurricane Conditions and Lessons Learned. J Perform Constr Facil 2020;34:04020102. https://doi.org/10.1061/(asce)cf.1943-5509.0001509.
[6] Pasch RJ, Penny AB, Berg R. National Hurricane Center Tropical Cyclone Report, Hurricane Maria; 2019. https://www.nhc.noaa.gov/data/tcr/AL152017_Maria.pdf.
[7] Cangialosi JP, Latto AS, Berg R. National Hurricane Center Tropical Cyclone Report: Huricane Irma. Natl Huricane Cent 2018:1–111. https://doi.org/10.1097/TA.0000000000002006.
[8] Blake ES, Zelinsky DA. National Hurricane Center Tropical Cyclone Report, Hurricane Harvey; 2018:1–77. https://www.nhc.noaa.gov/data/tcr/AL092017_Harvey.pdf.
[9] Alipour A, Aly AM, Davis BM, Soto MG, Kijewski-Correa T, Lenjani A, et al. Hurricane Michael preliminary virtual assessment team (p-vat) report; 2018. 10.17603/DS2G41M.
[10] Artemis. Hurricane Michael loss creeps to $7.2bn, but 17,347 claims still open; 2019: 1–2.
[11] Newmark C, (RMS). Hurricane Dorian Insured Losses in Caribbean from Wind, Storm-Surge; 2019. https://insurancejournal.com/news/international/2019/09/10/539310.htm.
[12] Jeworrek T. Record hurricane season and major wildfires – The natural disaster figures for 2020 2021. https://www.munichre.com/en/company/media-relations/media-information-and-corporate-news/media-information/2021/2020-natural-disasters-balance.html#1351999949.
[13] Behnken B, (NASA). 2020 Atlantic Hurricane Season. Cent Disaster Philanthr 2020. https://disasterphilanthropy.org/disaster/2020-atlantic-hurricane-season [accessed in March 2021].
[14] FEMA. Recommended Residential Construction for Coastal Areas: Building on Strong and Safe Foundations. http://fema.gov/library/viewRecord.do?id=1853 2009.
[15] Tomiczek T, Kennedy A, Rogers S. Survival analysis of elevated homes on the bolivar peninsula after hurricane IKE. Adv Hurric Eng Learn from Our Past – Proc 2012 ATC SEI Conf Adv Hurric Eng 2013:108–18. 10.1061/9780784412626.010.
[16] English EC, Friedland CJ, Orooji F. Combined Flood and Wind Mitigation for Hurricane Damage Prevention: Case for Amphibious Construction. J Struct Eng 2017;143:06017001. https://doi.org/10.1061/(ASCE)ST.1943-541X.0001750.
[17] Cochran L. Wind Issues in the Design of Buildings. Am Soc Civil Eng 2012. https://doi.org/10.1061/9780784412251.
[18] Amini M, Memari AM. Performance of Residential Buildings in Hurricane Prone Coastal Regions and Lessons Learned for Damage Mitigation. 5th Resid Build Des Constr Conf; 2020. https://www.researchgate.net/publication/340062711 Performance.
[19] MiraKijewski-Correa T, Alagusundaramoorthy P, Alsieedi M, Crawford S, Gartner M, Gutierrez Soto M, et al. StEER - Hurricane Dorian: Preliminary Virtual Reconnaissance Report (PVRR); 2019. 10.17603/ds2-saf8-4d32.
[20] Holmes JD. Wind pressures on tropical housing. J Wind Eng Ind Aerodyn 1994;53:105–23. https://doi.org/10.1016/0167-6105(94)90021-3.
[21] Amini M, Memari A. Evaluation of Various Retrofit Strategies for Existing Residential Buildings in Hurricane Prone Coastal Regions. 5th Resid Build Des Constr Conf; 2020. https://www.researchgate.net/publication/340062988 Evaluation.
[22] Abdelfatah N, Elawady A, Irwin P, Chowdhury AG. A study of aerodynamic pressures on elevated houses. Wind Struct An Int J 2020;31:335–50. https://doi.org/10.12989/was.2020.31.4.335.
[23] Kim JH, Moravej M, Sutley EJ, Chowdhury A, Dao TN. Observations and analysis of wind pressures on the floor underside of elevated buildings. Eng Struct 2020;221:111101. https://doi.org/10.1016/j.engstruct.2020.111101.
[24] Hoxey RP, Robertson AP, Richardson GM, Short JL. Correction of wind-tunnel pressure coefficients for Reynolds number effect. J Wind Eng Ind Aerodynam 1997;69–71:547–55. https://doi.org/10.1016/S0167-6105(97)00185-2.
[25] Hoxey RP, Robertson A, Richardson GM, Short JL. Observations of Reynolds number sensitivity in the separated flow region on a bluff body. J Wind Eng Ind Aerodyn 1998;73:231–49. https://doi.org/10.1016/S0167-6105(97)00287-0.
[26] Amini M, Memari AM. CFD-Based Evaluation of Elevated Coastal Residential Buildings under Hurricane Wind Loads. J Archit Eng 2021;in press:1–19. 10.1061/(ASCE)AE.1943-5568.0000472.
[27] American Society of Civil Engineering (ASCE). Minimum Design Loads and Associated Criteria for Buildings and Other Structures (ASCE/SEI 7-16); 2016. 10.1061/9780784412916.
[28] AS/NZS 1170.2. Australian and New Zealand wind loading standard, Structural design actions. Part 2, Wind actions. AS/NZS 11702 2011;2011:96.
[29] Chowdhury AG, Zisis I, Irwin P, Bitsuamlak G, Pinelli J-P, Hajra B, et al. Large-Scale Experimentation Using the 12-Fan Wall of Wind to Assess and Mitigate Hurricane Wind and Rain Impacts on Buildings and Infrastructure Systems. J Struct Eng 2017;143:04017053. https://doi.org/10.1061/(ASCE)ST.1943-541X.0001785.
[30] Chowdhury AG, Vutukuru K, Moravej M. Full- and Large-Scale Experimentation Using the Wall of Wind to Mitigate Wind Loading and Rain Impacts on Buildings and Infrastructure Systems. 11th Struct Eng Conv 2018.
[31] Choi CK, Kwon DK. Wind tunnel blockage effects on aerodynamic behavior of bluff body. Wind Struct An Int J 1998;1:351–64. https://doi.org/10.12989/was.1998.1.4.351.
[32] Irwin HPAH, Cooper KR, Girard R. Correction of distortion effects caused by tubing systems in measurements of fluctuating pressures. J Wind Eng Ind Aerodyn 1979;5:93–107. https://doi.org/10.1016/0167-6105(79)90026-6.
[33] ESDU (Engineering Sciences Data Unit). Characteristics of atmospheric turbulence near the ground Part III: variations in space and time for strong winds. vol. 9232; 2001, p. 1–42.
[34] Mooneghi MA, Irwin P, Chowdhury AG. Partial turbulence simulation method for predicting peak wind loads on small structures and building appurtenances. J Wind Eng Ind Aerodyn 2016;157:47–62. https://doi.org/10.1016/j.jweia.2016.08.003.
[35] Moravej M. Investigating scale effects on analytical methods of predicting peak wind loads on buildings. FIU Electronic Theses and Dissertations. 3799; 2018.
[36] Feng C, Gan Chowdhury A, Elawady A, Chen D, Azzi Z, Vutukuru KS. Experimental Assessment of Wind Loads on Roof-to-Wall Connections for Residential Buildings. Front Built Environ 2020;6:1–14. https://doi.org/10.3389/fbuil.2020.00010.
[37] Tominaga Y, Akabayashi S, Kitahara T, Arinami Y. Air flow around isolated gable-roof buildings with different roof pitches: Wind tunnel experiments and CFD simulations. Build Environ 2015;84:204–13. https://doi.org/10.1016/j.buildenv.2014.11.012.
[38] Gimenez JM, Bre F. Optimization of RANS turbulence models using genetic algorithms to improve the prediction of wind pressure coefficients on low-rise buildings. J Wind Eng Ind Aerodyn 2019;193:103978. https://doi.org/10.1016/j.jweia.2019.103978.
[39] Franke J, Hellsten A, Schlünzen H, Carissimo B. Best Practice Guideline for the CFD Simulation of Flows in the Urban Environment: COST Action 732 Quality Assurance and Improvement of Microscale meteorological models. Meteorol Model Meteorol Inst Univ Hamburg, Ger 2007;44:51.
[40] Versteeg HK, Malalasekera W. In: An Introduction to Computational Fluid Dynamics: The finite volume method. 2nd Ed. Harlow: Pearson Education; 2007. https://doi.org/10.1109/mcc.1998.736434.
[41] Amini M, Memari AM. LES simulations of wind - induced pressure on the floor system underside of elevated buildings. Wind Struct 2021;5:397–407.
[42] Xing F, Mohotti D, Chauhan K. Study on localised wind pressure development in gable roof buildings having different roof pitches with experiments, RANS and LES simulation models. Build Environ 2018;143:240–57. https://doi.org/10.1016/j.buildenv.2018.07.026.
[43] Jeong UY, Koh H-M, Lee HS. Finite element formulation for the analysis of turbulent wind flow passing bluff structures using the RNG k−ε model. J Wind Eng Ind Aerodyn 2002;90:151–69. https://doi.org/10.1016/S0167-6105(01)00190-8.
[44] Richards PJ, Hoxey RP. Appropriate boundary conditions for computational wind engineering models using the k-ϵ turbulence model. J Wind Eng Ind Aerodyn 1993;46–47:145–53. https://doi.org/10.1016/0167-6105(93)90124-7.
[45] Blocken B, Stathopoulos T, Carmeliet J. CFD simulation of the atmospheric boundary layer: wall function problems. Atmos Environ 2007;41:238–52. https://doi.org/10.1016/j.atmosenv.2006.08.019.
[46] Abdelfatah N, Elawady A. Numerical investigation of wind actions on elevated houses. 6th AAWE Work; 2021. p. 94–7. https://cecas.clemson.edu/wind/wp-content/uploads/2021/05/Proceedings-1.pdf.
[47] Singh J, Roy AK. CFD simulation of the wind field around pyramidal roofed single-story buildings. Springer Nat Switz 2019;1:1–10. https://doi.org/10.1007/s42452-019-1476-2.
[48] Menter FR. Zonal two equation k-w turbulence models for aerodynamic flows; 1993.